UCSF
UC San Francisco Previously Published Works

Title

Genomic characterization and therapeutic utilization of IL-13-responsive sequences in asthma

Permalink

https://escholarship.org/uc/item/7cs6d3x1

Journal

Cell Genomics, 3(1)

ISSN

2666-979X

Authors

Koh, Kyung Duk
Bonser, Luke R
Eckalbar, Walter L
et al.

Publication Date

2023

DOI

10.1016/j.xgen.2022.100229

Peer reviewed

eScholarship.org Powered by the California Digital Library
University of California

Cell Genomics

Article

Genomic characterization and therapeutic utilization of IL-13-responsive sequences in asthma

Graphical abstract

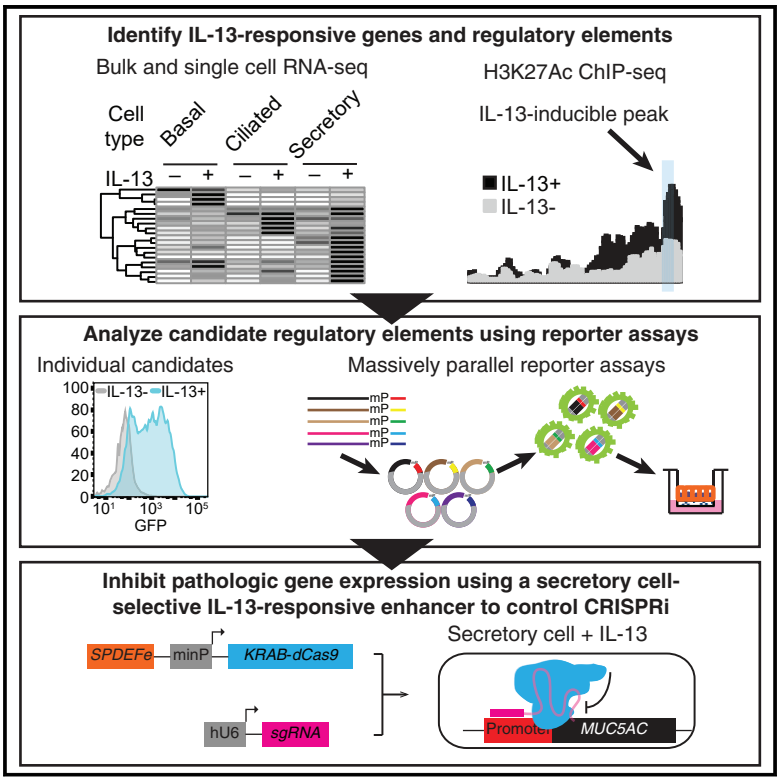

Highlights

- Genomic approaches identify airway epithelial regulatory elements important in asthma
- Integration of RNA-seq, H3K27ac ChIP-seq, and massively parallel reporter assays
- Discovery of an *SPDEF* enhancer driving secretory cell-selective responses to IL-13
- An enhancer-driven CRISPRi-mediated system prevented deleterious effects of IL-13

Authors

Kyung Duk Koh, Luke R. Bonser, Walter L. Eckalbar, ..., Walter E. Finkbeiner, Nadav Ahituv, David J. Erle

Correspondence

nadav.ahituv@ucsf.edu (N.A.), david.erle@ucsf.edu (D.J.E.)

In brief

Epithelial responses to the cytokine IL-13 cause airway obstruction in asthma. Koh et al. utilized scRNA-seq, H3K27ac ChIP-seq, and massively parallel reporter assays to identify IL-13-responsive regulatory elements in primary bronchial epithelial cells and develop a CRISPRi-based therapeutic agent to downregulate airway obstruction-inducing genes in a cell type- and IL-13-specific manner.

Koh et al., 2023, Cell Genomics *3*, 100229
January 11, 2023 © 2022 The Author(s).
https://doi.org/10.1016/j.xgen.2022.100229

CellPress

Cell Genomics

CellPress
OPEN ACCESS

Article

Genomic characterization and therapeutic utilization of IL-13-responsive sequences in asthma

Kyung Duk Koh,[1,2,7] Luke R. Bonser,[1,2,7] Walter L. Eckalbar,[1,3,7] Ofer Yizhar-Barnea,[2,4,7] Jiangshan Shen,[1,2] Xiaoning Zeng,[5] Kirsten L. Hargett,[2] Dingyuan I. Sun,[6] Lorna T. Zlock,[6] Walter E. Finkbeiner,[6] Nadav Ahituv,[2,4,*] and David J. Erle[1,2,3,8,*]

[1]Department of Medicine, University of California, San Francisco, San Francisco, CA 94143, USA
[2]Institute for Human Genetics, University of California, San Francisco, San Francisco, CA 94143, USA
[3]CoLabs, University of California, San Francisco, San Francisco, CA 94143, USA
[4]Department of Bioengineering and Therapeutic Sciences, University of California, San Francisco, San Francisco, CA 94158, USA
[5]Department of Pulmonary & Critical Care Medicine, The First Affiliated Hospital of Nanjing Medical University, Nanjing, China
[6]Department of Pathology, University of California, San Francisco, San Francisco, CA 94143, USA
[7]These authors contributed equally
[8]Lead contact
*Correspondence: nadav.ahituv@ucsf.edu (N.A.), david.erle@ucsf.edu (D.J.E.)
https://doi.org/10.1016/j.xgen.2022.100229

SUMMARY

Epithelial responses to the cytokine interleukin-13 (IL-13) cause airway obstruction in asthma. Here we utilized multiple genomic techniques to identify IL-13-responsive regulatory elements in bronchial epithelial cells and used these data to develop a CRISPR interference (CRISPRi)-based therapeutic approach to downregulate airway obstruction-inducing genes in a cell type- and IL-13-specific manner. Using single-cell RNA sequencing (scRNA-seq) and acetylated lysine 27 on histone 3 (H3K27ac) chromatin immunoprecipitation sequencing (ChIP-seq) in primary human bronchial epithelial cells, we identified IL-13-responsive genes and regulatory elements. These sequences were functionally validated and optimized via massively parallel reporter assays (MPRAs) for IL-13-inducible activity. The top secretory cell-selective sequence from the MPRA, a novel, distal enhancer of the sterile alpha motif pointed domain containing E-26 transformation-specific transcription factor (*SPDEF*) gene, was utilized to drive CRISPRi and knock down *SPDEF* or mucin 5AC (*MUC5AC*), both involved in pathologic mucus production in asthma. Our work provides a catalog of cell type-specific genes and regulatory elements involved in IL-13 bronchial epithelial response and showcases their use for therapeutic purposes.

INTRODUCTION

Asthma, a condition in which the airways narrow because of bronchoconstriction and excessive mucus production, affects ~262 million individuals worldwide.[1] Cytokine effects on the airway play a central role in asthma pathogenesis. Interleukin-13 (IL-13), interferon (IFN), and IL-17-stimulated gene expression is increased in subsets of individuals with asthma, and cytokine signatures are associated with disease severity, airway inflammatory responses, and responses to therapy.[2–4] These phenomena reflect pleiotropic effects of cytokines in the airway. For example, IL-13, which is implicated in at least half of individuals with asthma, induces eosinophilic inflammation,[5,6] airway smooth muscle hypercontractility,[7] fibroblast proliferation,[8] and mucus overproduction.[9,10] Using transgenic mice, we showed that direct effects of IL-13 on the airway epithelium are sufficient to induce two key features of asthma, mucus overproduction and airway hyperreactivity, in the absence of airway inflammation or fibrosis.[9] IL-13 stimulation of airway epithelial cells leads to formation of specialized secretory cells (goblet cells) that secrete mucin 5AC (MUC5AC), a major contributor to airway obstruction in asthma.[11] Studies in mice[12] and human epithelial cells[13] have demonstrated that this process depends on induction of the sterile alpha motif pointed domain containing E-26 transformation-specific transcription factor (SPDEF) in secretory cells.

Gene regulatory elements, such as promoters and enhancers, can contribute to cell type-specific responses.[14] These elements can be identified by genome-wide techniques, including chromatin immunoprecipitation sequencing (ChIP-seq) against histone modifications such as acetylated lysine 27 on histone 3 (H3K27ac).[15] Genome-wide technologies have been used to characterize cytokine responses, including macrophage responses to IL-4[16,17] and lung epithelial line responses to transforming growth factor β (TGF-β),[18] and the general epigenomic profile of undifferentiated human bronchial epithelial cells (HBECs).[19] However, more work is required to identify and functionally characterize IL-13-responsive elements in differentiated

This is an open access article under the CC BY-NC-ND license (http://creativecommons.org/licenses/by-nc-nd/4.0/).

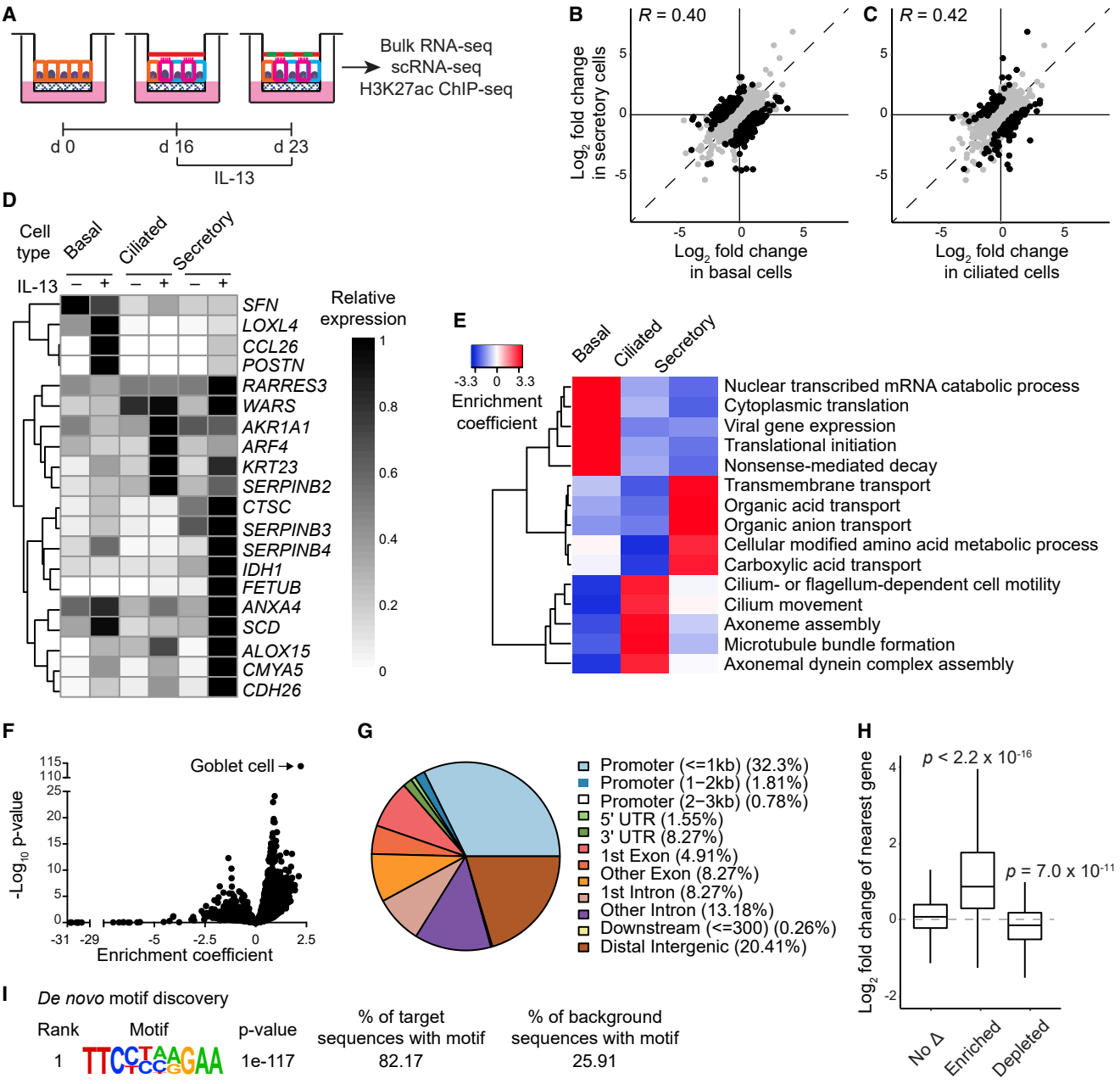

Figure 1. IL-13 induces cell-type-selective gene expression changes in each major subpopulation of bronchial epithelial cells, and enrichment of H3K27ac peaks near IL-13-stimulated genes

(A) Scheme for culturing primary human bronchial epithelial cells (HBECs) at an air-liquid interface (ALI) with IL-13 stimulation. On day 0, cells are predominantly basal cells (orange). ALI culture allows differentiation into ciliated (magenta) and secretory cells (cyan). The mucin 5B (MUC5B)-rich mucus gel layer (red) changes to a MUC5AC-rich gel (green) upon IL-13 stimulation.

(B and C) Effects of IL-13 on secretory cells compared with basal cells (B) or ciliated cells (C). Each point represents a gene. Genes that were regulated differently between cell types are shown in black ($\log_2$ fold change difference > 1 and FDR < 0.1 for interactions between cell type and cytokine effect), and other genes are shown in gray. *R*, Pearson correlation coefficient ($p < 2.2 \times 10^{-16}$ for both comparisons).

(D) Relative expression of 20 genes with the highest absolute IL-13-induced fold change in any of the three cell types.

(E) Gene set enrichment analysis of IL-13-induced cell type-selective responses in HBECs. Relative enrichment coefficients were calculated for the full collection of 2,555 gene ontology biological process (GOBP) gene sets; results are shown for the five GOBP gene sets that were most highly induced by IL-13 in basal, ciliated, and secretory cells ($p < 10^{-5}$ in one cell type and enrichment coefficient < 0.5 in other cell types).

(F) IL-13-induced genes in secretory cells are highly enriched for a previously defined set of goblet cell genes not included in GOBP. For comparison, unlabeled points represent values for the full collection of 2,555 GOBP gene sets.

(G) Distribution of IL-13-enriched H3K27ac peaks (N = 387) by genomic region classification.

(legend continued on next page)

HBECs. The development of massively parallel reporter assay (MPRA) technology allows simultaneous characterization of thousands of sequences and variants for their regulatory activity.[20] These regulatory elements could be used for therapeutic purposes by incorporating them into nuclease-deficient gene editing systems fused to transcriptional modulators, an approach called *cis* regulation therapy (CRT).[21]

Here we utilized multiple genomic methods (RNA sequencing [RNA-seq], H3K27ac ChIP-seq, and single-cell RNA-seq [scRNA-seq]) to characterize genes, regulatory elements, and pathways involved in IL-13 response in the airway epithelium, a complex tissue comprised of basal, ciliated, and secretory cells as well as other less common cell types. Previous studies have used some of these approaches in related systems. One previous study utilized scRNA-seq to identify cell type-specific effects of IL-13 stimulation on cultured human tracheal epithelial cells.[22] Another study[23] used H3K27ac profiling to compare the regulatory landscape of cells cultured from healthy control individuals and individuals with asthma, although these cells were cultured under conditions that do not promote cell differentiation, and the effects of IL-13 stimulation were not studied. Because there are important differences between the airway epithelial sample types used across these previous studies, we chose to use a single model that has been well characterized in our prior studies[11,13,24] to allow us to better associate gene expression and epigenetic changes. We then utilized MPRAs and individual reporter assays to identify IL-13-responsive regulatory elements. Using our top MPRA-derived element, a novel *SPDEF* enhancer shown to be IL-13 specific and secretory cell selective, we drove a CRISPR interference (CRISPRi)-based therapeutic approach to reduce the expression of critical asthma-associated genes. Our results identify key genes and regulatory elements in airway epithelial cells and demonstrate how enhancers can be used as therapeutic switches to treat disease.

RESULTS

Characterization of IL-13-responsive genes and pathways

We used scRNA-seq to identify IL-13 effects on primary HBECs (Figure 1A). HBECs grown in air-liquid interface (ALI) differentiate and recapitulate airway epithelial cell types seen *in vivo*, including ciliated and goblet cells.[25] HBECs from four individuals were grown in ALI for 16 days, and then half of the cultures were treated with IL-13 for 7 days to induce mucus hyperplasia.[11,13] Cells were harvested and utilized for scRNA-seq, yielding data for ~2,000 cells for each condition (Figures S1A–S1C). The proportions of cells classified as basal, ciliated, and secretory (Table S1) were consistent with our prior analyses of similar cultures by flow cytometry.[24]

Numerous genes were regulated by IL-13 (Figures 1B–1D; Table S7). To quantify cell type-selective effects, we used a linear model with terms for cell type, cytokine effect, and the interaction between the two. In this model, secretory cells were compared with each of the other two cell types. Cell type-specific effects of IL-13 were identified based on the interaction between IL-13 stimulation and cell type ($\log_2$ fold change difference > 1 and false discovery rate [FDR] < 0.1 for the interaction term). Cell type-specific effects were found for 292 genes in secretory cells compared with basal cells and 166 genes in secretory cells compared with ciliated cells. IL-13 affected different cellular processes in these three cell types (Figure 1E; Table S8). Examples of genes and pathways relevant to asthma that were selectively regulated in these cell types include periostin (*POSTN*) and serpin B2 (*SERPINB2*), two established markers of type 2-high asthma,[2] the pro-type 2 inflammatory genes C-C Motif Chemokine Ligand 26 (*CCL26,* an eosinophil chemoattractant) and arachidonate 15-lipoxygenase (*ALOX15*),[26] and genes involved in ciliated cell function and ion secretion. As expected, IL-13-induced transcripts in secretory cells were highly enriched for goblet cell genes defined previously in a scRNA-seq analysis of epithelial cells from human lungs[27] (Figure 1F).

We compared our results with those from a previous study of the effects of IL-13 stimulation on tracheal epithelial secretory cells.[22] Of the 200 genes we found to be most strongly induced by 7 days of IL-13 stimulation (fold increase > 1.98, FDR < 0.05), the previous study found significant increases for 71 genes after 48 h of IL-13 stimulation and 69 genes after 11 days of IL-13 stimulation (defined as fold change > 1.28, FDR < 0.05 in that study). In total, 103 of the 200 most highly induced genes in our study were induced at 48 h and/or 11 days in the previous study. Given differences in cell culture models (e.g., medium, IL-13 treatment duration) and scRNA-seq platforms, this represents a substantial overlap in the genes identified between studies. However, nearly half of the genes we identified as most highly induced by IL-13 were not identified in the prior study. *SPDEF*, a transcription factor shown previously to be required for goblet cell differentiation and MUC5AC production,[12,13,28] was among the 200 most highly IL-13-induced genes in secretory cells in our study (1.99-fold, FDR = 1.24×10^{-18}). Although *SPDEF* was not reported as significantly increased after 48 h or 11 days of IL-13 stimulation in the prior study, a pseudotime analysis of that prior dataset did indicate increased expression of *SPDEF* during goblet cell differentiation.[22] By applying scRNA-seq to the specific model system we characterized in our prior work, we identified many additional genes that were selectively induced by IL-13.

To analyze whether the cell type-specific response to IL-13 was a general cytokine response phenomenon or limited to IL-13, we generated similar scRNA-seq datasets for two other cytokines: IFN-α and IL-17. IFN-α produced a similar transcriptional response in each of the major cell types (Figures S1D,

(H) Bulk RNA-seq expression changes in genes closest to H3K27ac ChIP-seq peaks that were not significantly affected (p > 0.1) by IL-13 (no Δ, 26,875 peaks) or were significantly (FDR < 0.1) enriched (387 peaks) or depleted (215 peaks) after IL-13 stimulation. Shown are p values for comparison with unaffected peaks by two-sided Wilcoxon test.

(I) The most highly enriched motif discovered in regions with enriched H3K27ac after IL-13 stimulation closely resembles a previously defined STAT6 binding motif.

See also Figure S1 and Tables S1 and S7–S9.

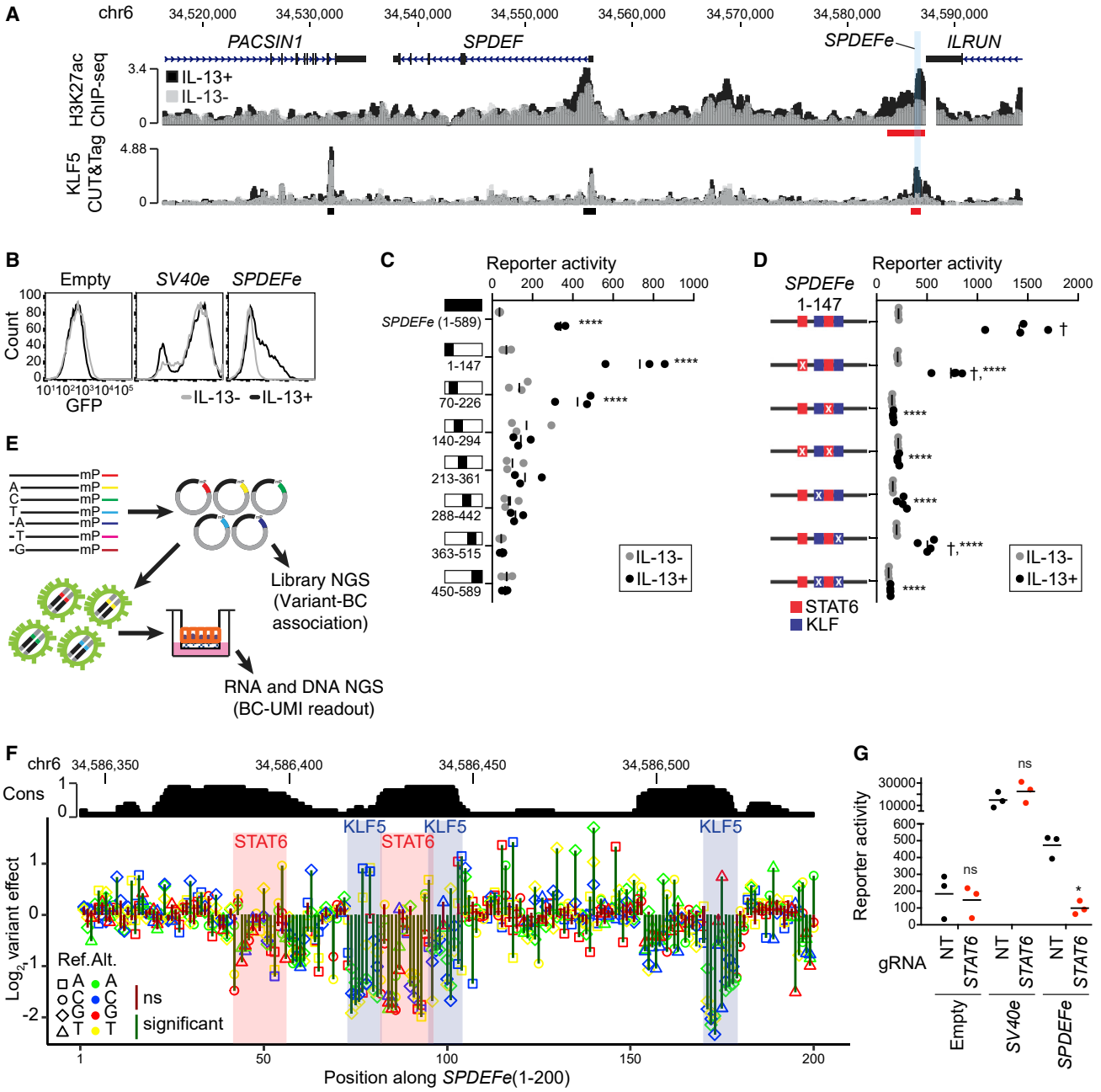

Figure 2. *SPDEFe* is IL-13 inducible, and its activity is mediated by STAT6 and KLF5

(A) IL-13 induces increased H3K27ac and KLF5 binding in a region 29 kb upstream of the *SPDEF* TSS. Top: overlaid tracks represent H3K27ac ChIP-seq read depth from HBECs cultured with (black) and without (gray) IL-13 stimulation (mean of four donors). The lone IL-13-regulated peak in this region is indicated by a red bar below the tracks (FDR < 0.1). An adjacent Encyclopedia of DNA Elements (ENCODE) blacklisted repetitive region that cannot be mapped reliably has been removed. Bottom: CUT&Tag analysis of KLF5 binding near the *SPDEF* locus. Tracks represent mean reads per million from six experiments (three donors, two replicates per donor) involving HBECs cultured without (gray) or with (black) IL-13 stimulation. Called peaks are indicated by bars below the tracks; the sole IL-13-enriched peak (FDR < 0.1) is shown in red. *SPDEFe* is highlighted in cyan.

(B) HBECs were transduced with lentiviral GFP reporter constructs containing only a minimal promoter (empty), a positive control SV40 enhancer (*SV40e*), or *SPDEFe* (chr6:34,586,344–34,586,932; hg38) and differentiated in ALI culture without (gray) or with (black) IL-13 stimulation during the last 7 days of culture. Representative histograms from one of at least three donors are shown.

(C) Seven overlapping ~150-bp fragments of *SPDEFe* from three donors were tested via the lentiviral GFP reporter assay in HBECs in ALI culture without (gray) or with (black) IL-13 stimulation. Values represent mean GFP reporter fluorescence intensity (arbitrary units). ****$p < 0.0001$ for comparison of IL-13 stimulation and no IL-13 stimulation by two-way ANOVA with Sidak's post-test.

(legend continued on next page)

S1E, and S1H). The interaction between IFN-α stimulation and cell type was significant ($\log_2$ fold-change difference > 1 and FDR < 0.1) for 58 genes in secretory cells compared with basal cells and 52 genes in secretory cells compared with ciliated cells; these cell type-selective differences were substantially less numerous than observed with IL-13. IL-17 response differed somewhat between these three cell types (Figures S1F, S1G, and S1I; significant interactions between IL-17 stimulation and cell type for 32 and 108 genes in secretory cells compared with basal and ciliated cells, respectively). We observed that all three cytokines had effects on gene expression, but IL-13 produced a substantially larger number of cell type-selective responses than IFN-α or IL-17.

Identification of IL-13-responsive DNA regulatory elements

To identify gene regulatory elements that are responsive to IL-13 in HBECs, we utilized ChIP-seq against H3K27ac, an active promoter and enhancer mark.[15,29] HBECs from four donors were grown in ALI with or without IL-13 stimulation (Figure 1A). Cells were harvested and crosslinked, and bulk H3K27ac ChIP-seq was performed. We identified 19,629 H3K27ac peaks; among these, 602 (3.1%, FDR < 0.1) were significantly changed by IL-13 stimulation (387 enriched, 215 depleted).

Analysis of genomic annotations of regions overlapping IL-13-responsive peaks from the ChIP-seq dataset found that approximately one-third contain putative promoters (Figure 1G). We analyzed these ChIP-seq peaks together with data from our bulk RNA-seq experiments of cytokine responses in ALI-cultured HBECs from six individuals (Table S9). Portions of the bulk RNA-seq data have been used previously to identify IFN signatures in bronchial samples from individuals with asthma and for analyses of regulation of severe acute respiratory syndrome coronavirus 2 (SARS-CoV-2)-related genes.[4,30] We evaluated the expression of the gene closest to a ChIP-seq peak and found that regions enriched in H3K27ac upon IL-13-stimulation were preferentially located near transcription start sites (TSSs) of IL-13-induced genes, as identified by bulk RNA-seq (Figure 1H). Conversely, regions depleted of H3K27ac in response to IL-13 tended to reside near genes with decreased expression. *De novo* motif analyses showed that the most highly enriched motif in IL-13-induced H3K27ac regions conforms to a signal transducer and activator of transcription 6 (STAT6) motif[31] (Figure 1I). These data indicate that IL-13-induced transcriptional changes correlate with changes in H3K27ac levels.

Identification and functional characterization of an IL-13-inducible *SPDEF* enhancer

We selected six IL-13-induced H3K27ac regions near three genes with known roles in asthma: PDIA5 protein disulfide isomerase family A member 5 (*PDIA5*), which is involved in the unfolded protein response and upregulated in allergic asthmatics;[32] *SPDEF*, which is a central mediator of goblet cell differentiation and involved in type 2 airway inflammation;[12,33] and Suppression Of Tumorigenicity 18 C2H2C-type zinc finger transcription factor (*ST18*), which is upregulated in atopic asthmatics.[34] We used a reporter assay to test activities of sequences from these regions in IL-13-stimulated, ALI-cultured HBECs (Figure S2). Among them, one 589-bp-long region located 29 kilobases (kb) upstream of the *SPDEF* TSS (Figure 2A), which we called *SPDEFe*, drove GFP-based reporter expression in an IL-13-dependent manner (Figure 2B). In contrast, our positive control, a constitutively active SV40 enhancer,[35] *SV40e*, produced reporter activity unaffected by IL-13 stimulation.

To further characterize *SPDEFe* and define the minimal active region, we tested overlapping ~150-bp fragments spanning the 589-bp sequence. Of seven constructs tested, only the first two, most proximal to *SPDEF* promoter, were active in IL-13-stimulated HBECs (Figure 2C). The first fragment, *SPDEFe*(1–147), encompassing the first 147 bp of the sequence and overlapping the second fragment, *SPDEFe*(70–226), provided the strongest response. According to the JASPAR database,[36] these two fragments include predicted binding sites for several transcription factors, including STAT6, which has a known role in IL-13 signaling.[37] Among those transcription factors, only Krüppel like factor 5 (*KLF5*) was significantly more abundant in secretory cells compared with basal and ciliated cells in our scRNA-seq (1.4- and 1.5-fold higher, respectively; FDR = 1.3×10^{-91} and 6.1×10^{-51}, respectively). We mutated the two STAT6 and two KLF5 predicted binding sites in *SPDEFe*(1–147) and repeated our reporter assay. Substituting nucleotides in the STAT6 or KLF5 binding sites reduced or eliminated IL-13-induced enhancer activity (Figure 2D). These findings demonstrate the requirement for STAT6 and KLF5 transcription factor binding sites within the 60-bp (44–103) region of *SPDEFe*.

Saturation mutagenesis MPRA identifies key factors regulating *SPDEFe*

To map the regions important for *SPDEFe* function at single-base-pair resolution, we used a saturation mutagenesis lentivirus-based MPRA (lentiMPRA) (Figure 2E). We generated a

(D) Mutations were made in core sequences of predicted STAT6 and KLF5 binding sites (JASPAR) in *SPDEFe*(1–147) and tested via the lentiviral GFP reporter assay in three donors. †$p < 0.0001$ for comparison of IL-13 stimulation and no IL-13 stimulation; ****$p < 0.0001$ for comparison with the reference *SPDEFe*(1–147) sequence by two-way ANOVA with Sidak's post-test. All other differences were not statistically significant (C and D).

(E) Scheme of the saturation mutagenesis lentivirus-based MPRA. Oligonucleotides containing each single-nucleotide variant *of SPDEFe*(1–200) were cloned into the lentiMPRA vector to create the plasmid library, which was sequenced to associate the sequence and its barcodes (BCs). The same plasmid library was used to prepare a lentivirus library that was subsequently transduced into HBECs, which were ALI cultured and treated with IL-13. RNA and DNA were harvested and sequenced to obtain BC and unique molecular identifier (UMI) counts.

(F) Saturation mutagenesis MPRA of bases 1–200 of *SPDEFe*. Values represent $\log_2$ effects of each single-nucleotide substitution (combined data from two donors). Positions of predicted STAT6 and KLF5 binding sites (JASPAR) are highlighted in red and blue, respectively. The extent of sequence conservation in 30 mammalian species by PhastCons is displayed at the top.

(G) Effects of *STAT6* targeting on reporter expression. HBECs from three donors were transfected with rCas9 and NT-2 control (black) or *STAT6* (red) guide RNA (gRNA) prior to introduction of the reporter constructs. ns, not significant; *$p < 0.05$ for comparison of NT-2 and *STAT6* gRNAs by Holm-Sidak t test.

See also Figures S2 and S3 and Table S10.

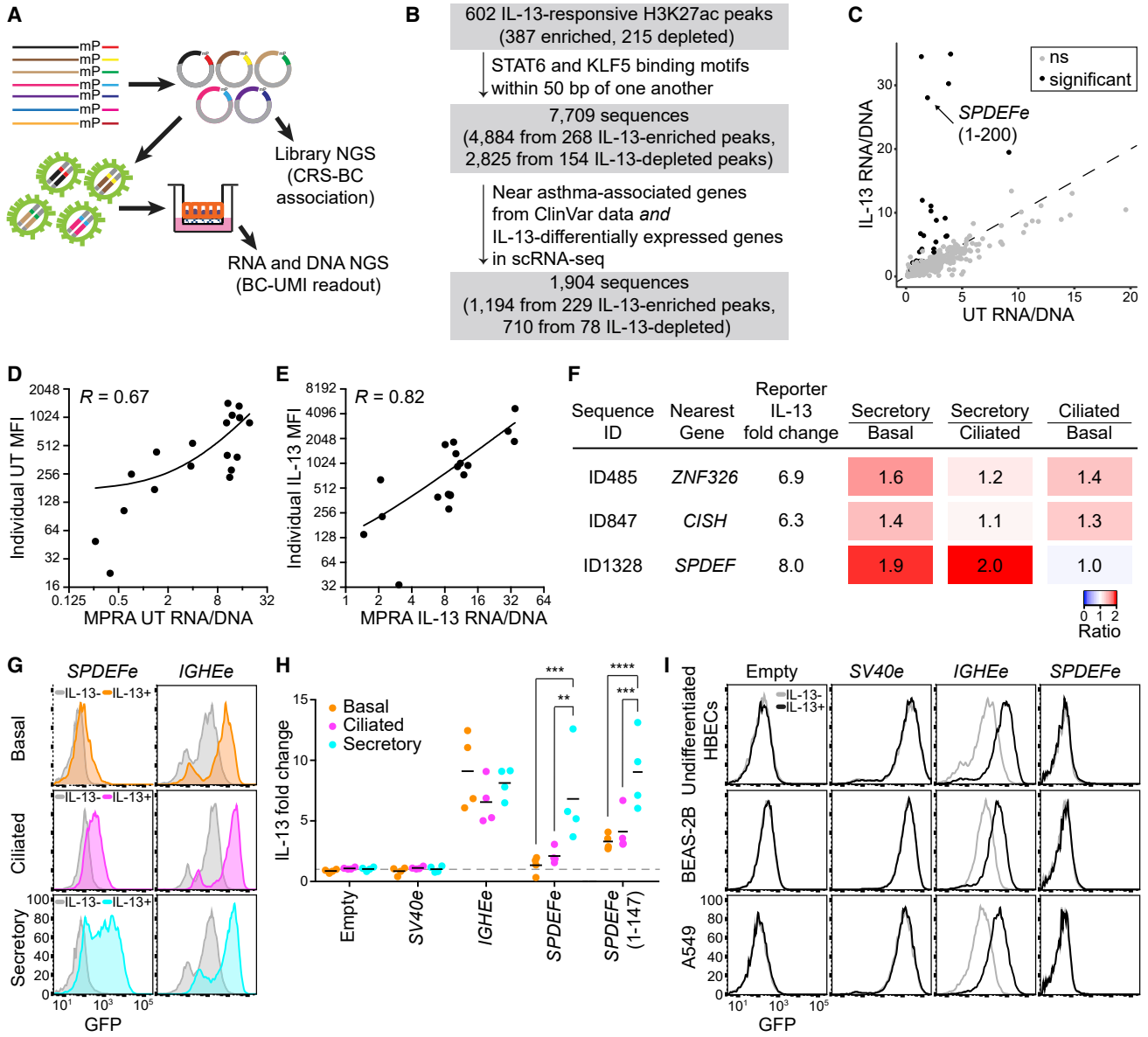

Figure 3. *SPDEFe* drives IL-13-inducible, cell type-selective transcription

(A) Scheme of the lentivirus-based MPRA. Oligonucleotides with each candidate *cis*-regulatory sequence (CRS) were cloned into the lentiMPRA vector to create the plasmid library, which was sequenced to associate the sequence and its BCs. A lentivirus library prepared from the plasmid library was transduced into HBECs, which were ALI cultured and treated with or without IL-13. RNA and DNA were harvested and sequenced for BC and UMI counts.

(B) Selection of 1,904 CRSs for the MPRA.

(C) MPRA results for CRSs. RNA/DNA ratios observed in untreated (UT) cells were plotted against those in IL-13-stimulated cells (combined data from two donors). IL-13-responsive CRSs are shown in black (>1.5-fold increase or decrease in IL-13 versus control, RNA/DNA ratio > 95th percentile of 100 scrambled negative control sequences, FDR < 0.1).

(D and E) Validation of 18 selected CRSs from the MPRA in HBECs. HBECs from a single donor were individually transduced with lentiviral GFP reporter constructs of CRSs differentiated in ALI culture without (gray) or with (black) IL-13 stimulation during the last 7 days of culture. Mean fluorescence intensity (MFI), measured by flow cytometry, was compared with RNA/DNA ratios from the MPRA. Pearson correlation coefficient ($p < 0.0001$).

(F) Reporter expression of the top three IL-13-inducible CRSs was measured in basal, ciliated, and secretory cells using a flow cytometry panel. "Reporter IL-13 fold change" represents the overall IL-13 effect seen in all cells. Cell type selectivity was quantified by taking the ratio of MFI in relevant cell types and normalizing it to the ratio observed for the empty construct.

(G and H) *SPDEFe*- and *IGHEe*-driven reporter expression in basal (nerve growth factor receptor [NGFR]$^+$ carcinoembryonic antigen-related cell adhesion molecule 6 [CEACAM6]$^-$), ciliated (acetylated α-tubulin [ac-α-Tub]$^+$), and secretory (CEACAM6$^+$ NGFR$^-$) cells. Shown are representative histograms from one of

(legend continued on next page)

library of 600 sequences covering all possible single-nucleotide variants of the first 200 bp of *SPDEFe* (Table S10). Oligonucleotides were synthesized and cloned into the lentiMPRA vector.[38] HBECs from two donors were transduced with the resulting lentivirus, ALI cultured with or without IL-13 stimulation, and harvested on day 23 of ALI culture. DNA and RNA were extracted, and enhancer activity was determined utilizing MPRAflow.[38] Analysis of our library showed a good correlation between donors (R = 0.77, $p < 2.2 \times 10^{-16}$; Figure S3A), and data were pooled for analysis.

Of the 600 tested mutations, 31 increased reporter expression and 128 reduced expression in IL-13-stimulated cells (absolute fold change $\geq$ 1.5, FDR < 0.05; Figure 2F). Function-perturbing mutations clustered at the previously identified STAT6 and KLF5 motifs and at a third KLF5 motif (positions 170–179), all of which are evolutionarily conserved across mammals (Figure 2F). Mutations in STAT6 and KLF5 motifs tended to have larger effects when they involved highly conserved positions, and mutations in the KLF5 motifs that increased similarity to the consensus motif tended to increase activity (Figures S3B–S3F). These results demonstrate that sequences containing STAT6 and KLF5 motifs are required for *SPDEFe* activity.

STAT6 and KLF5 regulate *SPDEFe*

To complement and validate our reporter assay results, we analyzed the functional interactions of STAT6 and KLF5 with *SPDEFe*. We used CRISPR to target *STAT6* in HBECs and observed an editing efficiency of more than 90%, as measured by PCR, Sanger sequencing, and inference of CRISPR edits (ICE) analysis.[39] Cells were then transduced with the *SPDEFe* reporter, grown in ALI culture, and treated with IL-13 or left untreated. We observed that CRISPR-mediated deletion of STAT6 prevented IL-13-induced activation of the *SPDEFe* reporter (Figure 2G). We found that CRISPR targeting of *KLF5* in HBECs leads to cell death upon ALI culture, consistent with a previous study showing that *Klf5* is required for airway epithelial maturation in mice.[40] Consequently, we analyzed KLF5's ability to bind to *SPDEFe* using cleavage under targets and tagmentation (CUT&Tag).[41] HBECs from three donors were grown in ALI and treated with IL-13 or left untreated, followed by CUT&Tag. We identified 22,948 CUT&Tag KLF5 peaks (KLF5 motif as the most highly enriched in peaks; $p = 10^{-1306}$). *SPDEFe* is located in one of 863 regions that more strongly associated with KLF5 after IL-13 stimulation (FDR < 0.1; Figure 2A). We also attempted to identify STAT6 binding sites directly using CUT&Tag, but an antibody used previously for STAT6 ChIP-seq[16,42] is no longer available, and attempts to use two other commercially available STAT6 antibodies were unsuccessful. The results of our *SPDEFe* mutational analyses combined with the STAT6 targeting studies and the KLF5 CUT&Tag findings support the hypothesis that *SPDEFe* is activated by STAT6 and KLF5 in HBECs after IL-13 treatment.

Massively parallel characterization of IL-13-responsive gene regulatory elements

Because STAT6 and KLF5 were vital for the IL-13-inducible activity of *SPDEFe*, we hypothesized that STAT6/KLF5-dependent, IL-13-responsive elements likely contributed to IL-13-regulated gene expression in HBECs. To this end, we performed a lentiMPRA (Figure 3A). Because of the biological constraints involved in growing HBECs, which provide only a limited number of cells and passages, we limited the amount of candidate *cis*-regulatory sequences (CRSs) tested in our MPRA using the following criteria (Figure 3B): (1) IL-13-responsive peaks in our H3K27ac ChIP-seq data that contain STAT6 and KLF transcription factor binding motifs within 50 bp of each other, (2) proximity to asthma-associated genes (established according to ClinVar data), and (3) proximity to IL-13 differentially expressed genes in our scRNA-seq data. A total of 1,194 CRSs from IL-13-enriched H3K27ac peaks and 710 CRSs from IL-13-depleted H3K27ac peaks were selected using these criteria (Table S11). We used *SV40e* and *SPDEFe*(1–200) sequences as positive controls and scrambled versions of 100 randomly selected CRSs as negative controls.

Oligonucleotides for this library were cloned into a lentiMPRA vector, and HBECs from the same two donors used in the *SPDEFe*(1–200) saturation mutagenesis MPRA were transduced and ALI cultured with or without IL-13 treatment. On day 23 of ALI culture, DNA and RNA were extracted, sequenced, and analyzed using MPRAflow.[38] We observed a good correlation between the two donors (R = 0.87 and 0.88, $p < 2.2 \times 10^{-16}$ for untreated and IL-13 treatment conditions, respectively; Figure S4) and therefore pooled the results for analysis.

Of the 1,194 CRSs in IL-13-enriched H3K27ac peaks, 26 CRSs met our criteria for induced expression after IL-13 treatment (IL-13 fold change > 1.5, IL-13 RNA/DNA > 95th percentile for 100 randomized negative control sequences, FDR < 0.1; Figure 3C; Table S11). The top IL-13-induced sequence was ID1328, which harbors *SPDEFe* (positions 1–179; IL-13 fold change of 25). Only one of the 710 CRSs derived from IL-13-depleted H3K27ac regions led to significantly repressed expression by IL-13 (IL-13 fold change < 0.67, untreated [UT] RNA/DNA > 95th percentile for 100 randomized negative control sequences, FDR <0.1).

We next validated our MPRA results by testing 18 individual sequences for reporter activity in HBECs (Table S11). We selected 5 classified as IL-13 inducible (IL-13 fold change > 3 and FDR < 0.1), 2 showing inconsistent results in two donors, and 11 that were not IL-13 inducible but led to high reporter expression regardless of condition (RNA/DNA > 5 in UT and IL-13). Lentiviral reporters containing these sequences were introduced into HBECs, and the cells were grown in ALI culture with or without IL-13 and analyzed for reporter expression via flow cytometry. We observed a good correlation with the MPRA results (R = 0.67 and 0.82 for UT and IL-13, respectively;

four donors (G) and IL-13-induced fold changes in reporter expression (MFI) in each cell type (H). **p < 0.01, ***p < 0.001 for comparison between cell types by two-way ANOVA Tukey's post-test; all other differences were not statistically significant.

(I) Reporter activity in undifferentiated HBECs and two lung epithelial cell lines, BEAS-2B and A549. Representative histograms from at least three donors or experiments are shown.

See also Figures S4–S6 and Table S11.

$p < 0.0001$; Figures 3D and 3E). Of the four sequences that were most highly induced in the MPRA, three showed similar IL-13-inducible response in this validation experiment. These sequences were analyzed for cell type-specific activation by dissecting reporter expression using a panel of cell type-specific markers.[24] Only one sequence, ID1328, harboring *SPDEFe*(1–179), was found to be substantially cell type selective in secretory cells (Figure 3F).

SPDEFe is activated by IL-13 selectively in secretory cells

Examination of our scRNA-seq data showed that IL-13 stimulation induces *SPDEF* expression specifically in secretory cells (1.99-fold, FDR = 1.24×10^{-18}; Table S7), whereas its expression in basal and ciliated cells was >10-fold lower and minimally affected (<1.1-fold) by IL-13. To assess whether *SPDEFe* confers cell type selectivity, we assayed its activity in HBECs from four additional donors. The activity of *SPDEFe* was significantly induced by IL-13 only in secretory cells, whereas a constitutively active *SV40e* exhibited no IL-13 inducibility or cell type selectivity (Figures 3G, 3H, and S5A). The shorter fragment of *SPDEFe* with essential STAT6 and KLF5 motifs (*SPDEFe*(1–147)) also led to high IL-13 inducibility while maintaining secretory cell selectivity (Figure 3H). To assess whether *SPDEFe*'s selectivity reflects a general difference in activation of the IL-13/STAT6 signaling pathway between cell types, we tested a reporter construct containing a germline immunoglobulin heavy constant epsilon promoter (*IGHEe*). *IGHEe* contains previously characterized STAT6 and CEBPβ binding sites and has a known role in IL-4-induced, STAT6-mediated B cell immunoglobulin class switching.[43] We cloned *IGHEe* into a reporter lentivirus, transduced it into HBECs, ALI-cultured cells with or without IL-13 stimulation, and measured reporter expression. IL-13 induced *IGHEe* activity in all cell types, demonstrating that the selectivity of *SPDEFe* is not attributable to difference in activation of the STAT6 pathway between cell types (Figures 3G, 3H, and S5B).

To assess the dependence on cell differentiation, we transduced HBECs that were maintained in standard (submerged) cell culture, where cells remain in a poorly differentiated state, and two epithelial cell lines, BEAS-2B and A549, commonly used in *in vitro* experiments on lung biology, with *IGHEe* or *SPDEFe*. IL-13 activated *IGHEe* but not *SPDEFe* in all cell types (Figure 3I). These findings suggest that *SPDEFe* is an IL-13-dependent enhancer that is selectively active in differentiated secretory cells.

SPDEFe is activated by IL-13 but not by other stimuli that promote mucin production

We next sought to determine whether *SPDEFe* is specifically activated by IL-13. MUC5AC overproduction is detrimental in asthma, and its downregulation could potentially be used as a therapeutic strategy. Because *MUC5AC* is minimally expressed in unstimulated HBECs under our ALI culture conditions, we used an alternative cell culture medium, PneumaCult-ALI, which supports development of MUC5AC-producing cells without a requirement for IL-13 stimulation, as seen *in vivo*.[44] HBECs cultured in PneumaCult-ALI and transduced with the *SPDEFe* reporter produced MUC5AC but did not activate *SPDEFe* (Figures S6A and S6B). *MUC5AC* expression is also induced by IL-1β in the context of airway infection.[45] Providing IL-1β to HBECs transduced with the *SPDEFe* reporter and grown under ALI culture conditions also did not activate *SPDEFe* (Figures S4C and S4D). These results suggest that *SPDEFe* activation is selective for IL-13 as opposed to other *MUC5AC*-inducing stimuli.

CRISPRi implicates *SPDEFe* as a regulator of SPDEF-dependent goblet cell differentiation and mucus hyperplasia

CRISPRi has been used to test whether candidate loci function as gene regulatory regions in various cell types, including lung cells.[46] We used CRISPRi (Figure 4A) to validate that *SPDEF* is the target gene for *SPDEFe* and determine whether *SPDEFe* downregulation can reverse IL-13-induced, asthma-associated abnormalities in mucus organization and function. We designed four gRNAs targeting *SPDEFe*, the *SPDEF* promoter, or the *MUC5AC* promoter and cloned them into a lentivirus-based single-guide RNA (sgRNA) vector. As a negative control, we used previously published non-targeting guide RNAs (gRNAs).[47] HBECs from a single donor were co-transduced with sgRNA vectors and a vector that drives expression of nuclease-deficient Cas9 (dCas9) fused to the Krüppel associated box (KRAB) transcriptional repressor. Cells were grown in ALI with or without IL-13 treatment, and RNA was isolated from these cells and used to measure gene expression. For cells with control, non-targeting sgRNAs, we observed IL-13 induction of *SPDEF* and the SPDEF-regulated genes forkhead box A3 (*FOXA3*) and *MUC5AC* (Figures 4B–4D). CRISPRi targeting of the *MUC5AC* promoter reduced *MUC5AC* mRNA by 60% but did not affect *SPDEF* or *FOXA3*, which are upstream of *MUC5AC*. In contrast, targeting the *SPDEF* promoter reduced *SPDEF* (65%), *FOXA3* (67%), and *MUC5AC* (72%) mRNA levels as well as MUC5AC protein (65% as measured by flow cytometry; Figures 4B–4E). CRISPRi targeting of *SPDEFe*, similar to targeting the *SPDEF* promoter, reduced *SPDEF* (64%), *FOXA3* (66%), and *MUC5AC* (64%) mRNA expression and MUC5AC protein (60%), implicating *SPDEF* as its target gene. Each of the four *SPDEFe*-targeting gRNAs had similar effects on expression of *SPDEF* and SPDEF-regulated genes, and these effects were not seen with negative control gRNAs, indicating that the effects of targeting *SPDEFe* were specific. We also measured the effects of targeting *SPDEFe* on expression of the other major airway mucin, *MUC5B*, which is known to be regulated by SPDEF.[13,48] IL-13 decreased *MUC5B* expression, as expected from prior studies,[11,13] and targeting the *SPDEF* promoter or *SPDEFe* further decreased *MUC5B* expression (Figure S7A).Targeting the *MUC5AC* promoter in IL-13-stimulated cells increased *MUC5B* expression to a level similar to that seen in unstimulated cells. More studies are required to determine whether this results from a compensatory mechanism to maintain mucin expression or a complex regulatory interaction within the chromosome 11p15 cluster containing *MUC5AC* and *MUC5B*. Our results show that CRISPRi targeting of *SPDEFe* specifically inhibits expression of *SPDEF* and SPDEF-regulated genes, including *FOXA3*, *MUC5AC*, and *MUC5B*.

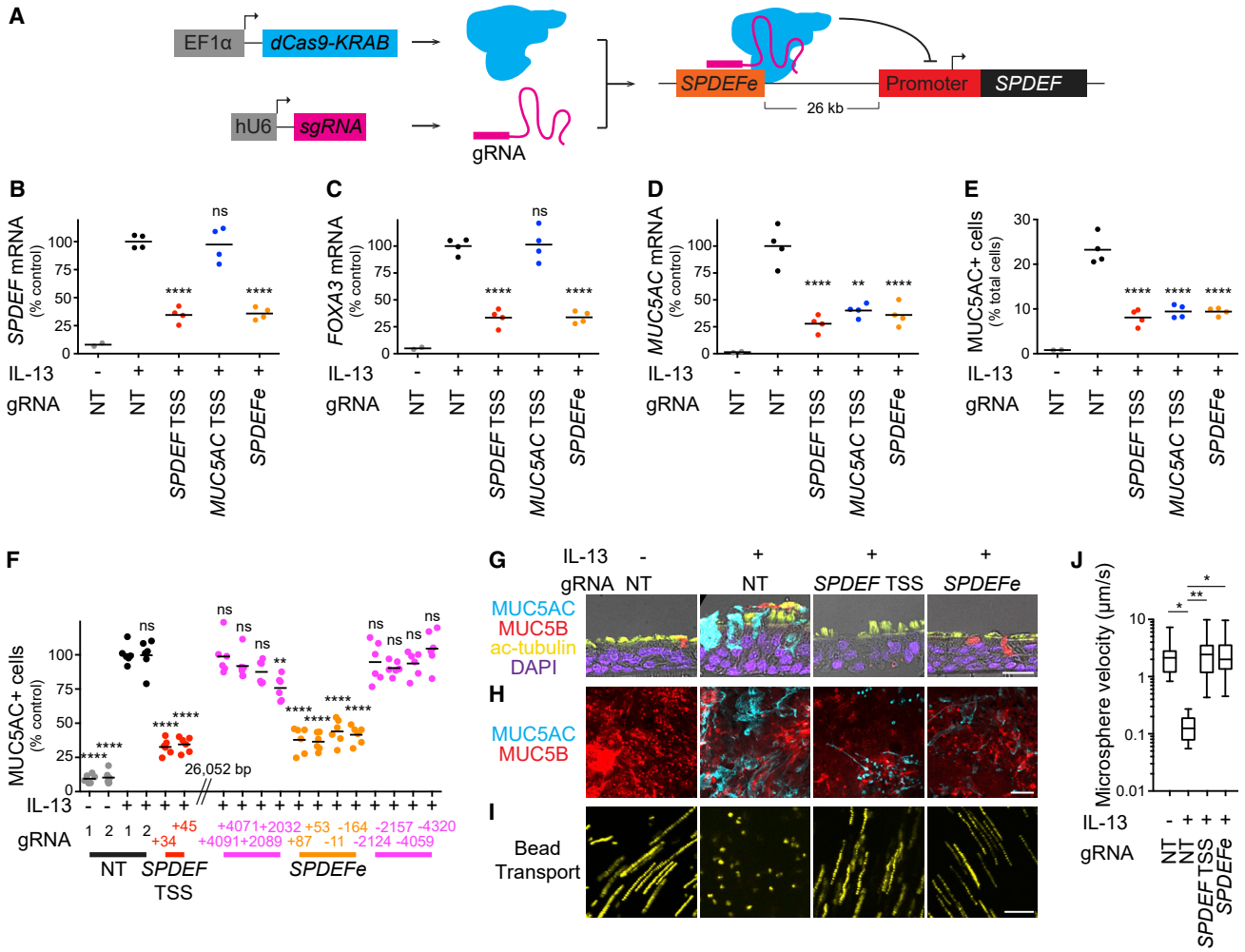

Figure 4. CRISPRi targeting of the *SPDEF* enhancer prevents SPDEF-dependent, IL-13-induced mucus metaplasia and mucostasis

(A) Scheme of CRISPRi targeting of *SPDEFe*.

(B–D) CRISPRi effects on gene expression. HBECs were transduced with lentiviruses driving expression of *dCas9-KRAB* and non-targeting (NT) control sgRNAs (gray/black) or sgRNAs targeting the *SPDEF* promoter (red), *MUC5AC* promoter (blue), or *SPDEFe* (orange). After differentiation, cells were left unstimulated or stimulated with IL-13 for 7 days, as indicated. Expression of *SPDEF* (B), *FOXA3* (C), and *MUC5AC* (D) was measured by quantitative real-time PCR. mRNA levels are relative to IL-13-stimulated HBECs with NT control sgRNAs.

(E) CRISPRi effects on intracellular MUC5AC were quantified by flow cytometry. Each point corresponds to a different gRNA targeting the indicated region, tested separately in a single culture well from the same donor (B–E). $^{**}p < 0.01$, $^{****}p < 0.0001$ for comparison with IL-13-stimulated HBECs with NT control sgRNAs by one-way ANOVA with Dunnett's post-test (B–E).

(F) Effects of targeting *SPDEFe* and surrounding regions on IL-13-induced MUC5AC production. gRNAs used in (B)–(E) were compared with gRNAs targeting flanking regions ~2 and 4 kb away from *SPDEFe* (magenta) in a separate set of experiments (three donors, two replicates per donor). To combine results from two donors, values for MUC5AC-producing cells are shown as percentages of mean values for IL-13-stimulated cells with NT sgRNAs in the same donor. $^{**}p < 0.01$, $^{****}p < 0.0001$ compared with IL-13-stimulated HBECs with NT-1 sgRNA by one-way ANOVA with Tukey's post-test. p values for all comparisons are provided in Table S2.

(G–J) CRISPRi effects on mucin staining and mucociliary transport. HBECs were treated as above using NT-2 gRNA, *SPDEF*-TSS(+34) gRNA, or *SPDEFe*(+87) gRNA. Sections (G) and extracellular mucus gels from whole-mount preparations (H) were stained for MUC5AC (cyan), MUC5B (red), and the ciliated cell marker ac-α-Tub (yellow). Nuclei were stained with DAPI (purple). Scale bars: 20 μm (G) and 100 μm (H). Images are representative of two experiments with different donors. Mucociliary transport rates were determined from trajectories of fluorescent microspheres placed on gels atop cells (I and J). Shown is superimposition of 10 images acquired at 1-s intervals; scale bars: 50 μm (I). Microsphere speeds were determined from three donors, one well per donor, four fields per well (J). Values represent median microsphere speed for each field. Boxes extend from the 25th to the 75th percentile, horizontal lines within the box indicate means, and whiskers represent minimum and maximum values. $^{*}p < 0.05$, $^{**}p < 0.01$ by one-way ANOVA with Tukey's post-test.

See also Figures S7 and S8 and Table S2.

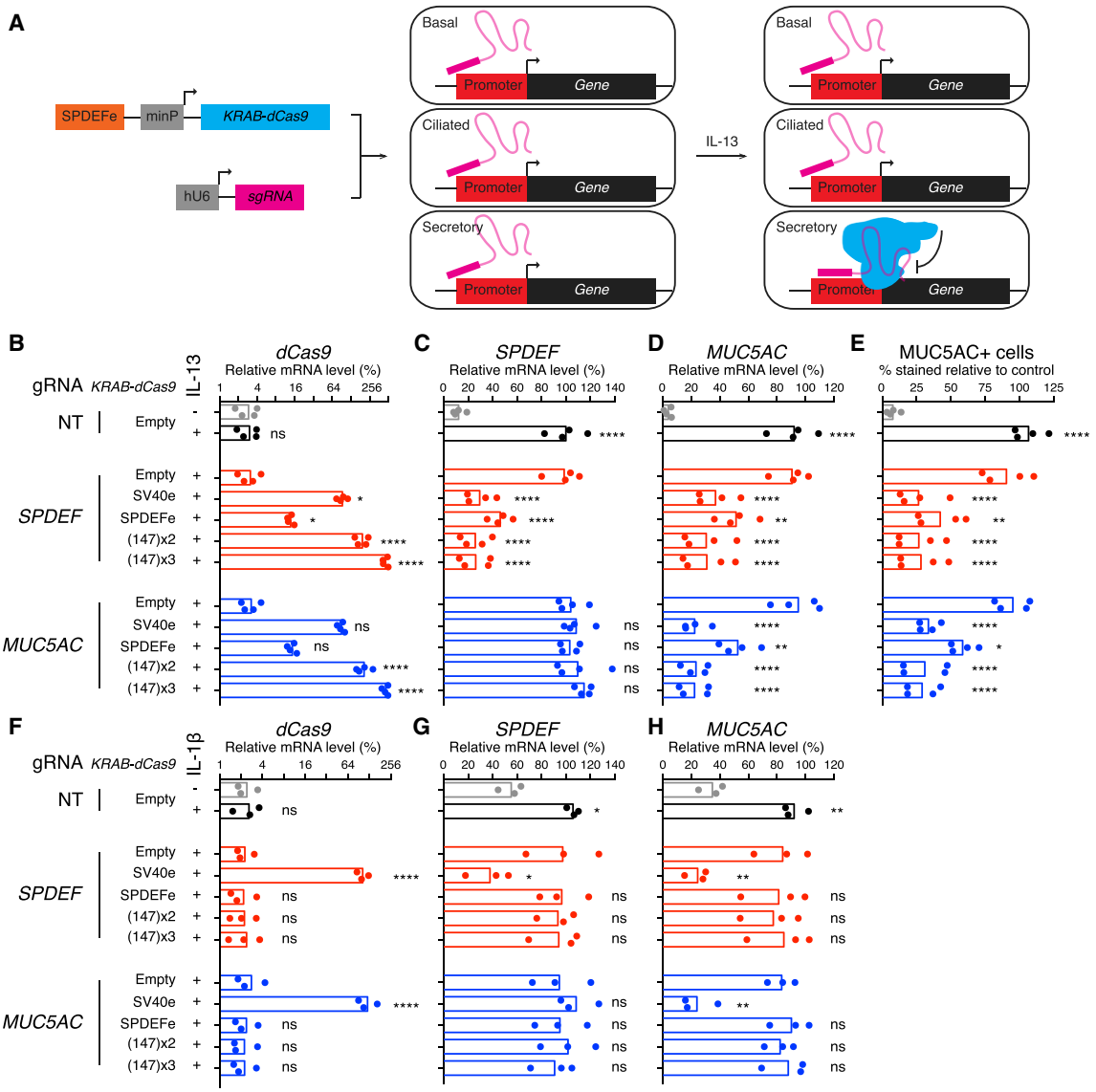

Figure 5. *SPDEFe* can be used to drive CRISPRi to prevent IL-13-induced mucin production by secretory cells

(A) Scheme of IL-13-responsive, secretory cell-specific, *SPDEFe*-driven CRISPRi. minP, minimal promoter.

(B–H) A lentivirus containing a *KRAB-dCas9* transgene driven by *SPDEFe* (or other enhancers) and a second lentivirus driving expression of sgRNA targeting the *SPDEF* (SPDEF-TSS(+34)) or *MUC5AC* (MUC5AC-TSS(+134)) promoter were used in combination. Transduced cells were ALI cultured without cytokine stimulation or with IL-13 (B–E) or IL-1β (F–H) stimulation for the last 7 days of culture, as indicated. Changes in expression of *dCas9* (B and F), *SPDEF* (C and G), and *MUC5AC* (D and H) were measured by quantitative real-time PCR. MUC5AC-producing cells (E) were quantitated by flow cytometry. mRNA levels and MUC5AC-producing cells are relative to mRNA levels and MUC5AC-producing cells from IL-13-stimulated cells with *SV40e-KRAB-dCas9* and NT-2 sgRNA in the same donor. IL-13 data (B–E) are from four donors. The IL-1β data (F–H) are from cells from three donors, including two used for the IL-13 experiment. *$p < 0.05$, **$p < 0.01$, ****$p < 0.0001$ compared with the unstimulated empty vector control for NT gRNA and IL-13-stimulated empty vector control for *SPDEF* and *MUC5AC* gRNAs by one-way ANOVA Tukey's post-test (B–H).

To exclude the possibility that targeting *SPDEFe* has non-specific effects on IL-13 responsiveness, we measured expression of periostin (*POSTN*), a gene frequently used as part of an IL-13-response signature in asthma.[2] Targeting the *SPDEF* promoter or *SPDEFe* had no effects on this IL-13-inducible gene or on expression of the basal cell marker *KRT5* and the ciliated cell marker *TUBB4B* (Figures S7B–S7D). These results suggest that CRISPRi targeting of the *SPDEF* promoter or *SPDEFe* does not affect responsiveness to IL-13 or differentiation of HBECs. To look for off-target effects, we analyzed the expression of neighboring genes (*HMGA1*, *NUDT3*, *ILRUN*, *SNRPC*, and *FKBP5*) in the same topologically associated domain (TAD) as *SPDEF*, according to Hi-C data from a lung epithelial cell line, A549,[49] and human tracheobronchial epithelial cells.[50] We

observed no significant IL-13-induced changes in expression of these genes (Figures S7E–S7I), although we cannot exclude modest effects (~80% power to detect a 1.7-fold change for each gene tested). This suggests that CRISPRi targeting of *SPDEFe* using these gRNAs has modest, if any, effects on neighboring gene expression in the same TAD. To pinpoint the location of *SPDEFe*, we performed an additional experiment using HBECs from three donors and found that gRNAs targeting *SPDEFe* again suppressed MUC5AC induction, whereas sequences 2–4 kb from *SPDEFe* had minimal effects (Figure 4F; Table S2). These results indicate that CRISPRi against *SPDEFe* effectively and selectively suppresses IL-13-induced *SPDEF* and SPDEF-dependent genes. As a complementary approach, we used a pair of flanking gRNAs in combination with catalytically active Cas9 to excise *SPDEFe* from the genome. Excising *SPDEFe* significantly reduced levels of *SPDEF* mRNA and the SPDEF-dependent genes *FOXA3* and *MUC5AC* (Figure S8), providing evidence that *SPDEFe* regulates *SPDEF* expression.

We next analyzed whether CRISPRi targeting of *SPDEFe* reverses IL-13-induced abnormalities in mucus organization and function associated with asthma. IL-13 stimulation induces formation of MUC5AC-rich mucus that remains tethered to the epithelium, resulting in impaired mucociliary transport.[11] Consistent with our analyses of the effects of *SPDEFe* gRNAs on *MUC5AC* mRNA and MUC5AC protein by flow cytometry, we found that CRISPRi targeting of *SPDEFe* prevented formation of MUC5AC-rich mucus domains (Figures 4G and 4H). We investigated whether targeting *SPDEFe* via CRISPRi could also rescue mucociliary transport abnormalities induced by IL-13. As expected, IL-13 stimulation of cells expressing a non-targeting sgRNA led to a marked reduction in mucociliary clearance.[11] In contrast, targeting the *SPDEF* TSS or *SPDEFe* completely rescued IL-13-induced mucostasis (Figures 4I and 4J). These results show that direct targeting of *SPDEFe* prevents IL-13 induction of *SPDEF* and the goblet cell transcriptional program and impaired mucociliary clearance.

SPDEFe-driven CRISPRi inhibits asthma-associated genes in an IL-13-dependent, cell type-specific manner

Our previous experiments suggest that *SPDEFe* could be utilized as an exceptional regulatory switch that could be specifically turned on by IL-13 in differentiated secretory cells, providing a therapeutic driver to precisely alter gene expression in asthma. To examine this, we cloned *SPDEFe* in front of *KRAB-dCas9* and tested its ability to reduce *SPDEF* or *MUC5AC* gene expression in differentiated secretory cells after IL-13 stimulation (Figure 5A). *SPDEFe-KRAB-dCas9* lentiviruses were transduced into HBECs from four donors together with lentiviruses encoding sgRNAs targeting the *SPDEF* or *MUC5AC* TSS. After ALI culture and treatment with or without IL-13, we observed that *SPDEFe* in combination with the *SPDEF*-targeting sgRNA drove expression of *KRAB-dCas9* in an IL-13-inducible manner and significantly reduced *SPDEF* and *MUC5AC* expression and MUC5AC protein level (Figures 5B–5E). With the *MUC5AC*-targeting sgRNA, *MUC5AC*/MUC5AC expression was reduced without affecting *SPDEF* expression (Figures 5B–5E), as expected, because *SPDEF* is upstream of *MUC5AC*. We next tested whether increasing the number of *SPDEFe* copies can further increase the magnitude of CRISPRi downregulation. We generated CRISPRi vectors with sequences containing two or three copies of *SPDEFe*(1–147) and observed that increasing the number of copies increased *dCas9* expression (Figure 5B) and reduced *SPDEF* and *MUC5AC* mRNA levels (Figures 5C and 5D) as well as MUC5AC protein levels (Figure 5E), with two copies having a similar effect as three copies.

To validate that *SPDEFe* is IL-13 specific, we performed these experiments using IL-1β, another MUC5AC-inducing cytokine, instead of IL-13. IL-1β did not induce expression of *KRAB-dCas9* (Figure 5F), and *SPDEFe*-driven CRISPRi did not prevent IL-1β induction of *SPDEF* and *MUC5AC* (Figures 5G and 5H). Our results show that *SPDEFe* can be used as a regulatory switch to specifically modulate gene expression in an IL-13-induced manner in differentiated airway secretory cells.

DISCUSSION

The ability to control gene expression in a cell type-selective and cytokine-inducible manner could allow specific control of genes and transcriptional modulators to treat asthma. Here we utilized numerous genomic technologies (scRNA-seq, H3K27ac ChIP-seq, and MPRAs) to identify an enhancer, *SPDEFe*, that is activated by IL-13 specifically in differentiated secretory bronchial epithelial cells. We show that downregulating the activity of this enhancer via CRISPRi or utilizing it to drive CRISPRi can provide therapeutic benefits for asthma treatment.

Cytokines such as IL-13 are known to have distinctive effects on HBECs in individuals with asthma.[2–4] As observed in our scRNA-seq data, IL-13 has cell type selectivity and, in secretory cells, induces genes associated with goblet cell hyperplasia, a process that transforms the histological appearance and secretome of these cells. Goblet cells are the source of tethered MUC5AC, which impairs mucociliary clearance and causes airway obstruction.[11] A previous study focusing on IL-13 effects on human tracheal epithelial cells also showed substantial cell type-specific effects.[22] In basal cells, IL-13 selectively induced genes encoding eotaxin-3 (CCL26), which recruits eosinophils,[51] and periostin, a pro-fibrotic and anti-inflammatory matricellular protein[52] that has been used as a marker for type 2-high asthma.[2] *SERPINB2*, another type 2-high asthma marker, was among the genes most highly induced in ciliated cells (Figure 1D). IL-13 has distinct effects even in epithelial cells from a single tissue, and these cell type-selective effects contribute to different features of asthma.

To identify regulatory elements that control the cell type-selective effects of IL-13 on gene expression, we utilized H3K27ac ChIP-seq. IL-13 induced numerous changes in H3K27ac, many of which were associated with increased expression of nearby genes, suggesting a functional role. We used these data to guide our individual reporter assays and MPRA experiments. Although most CRSs identified by H3K27ac ChIP-seq were not active in the MPRA, the ability of the MPRA to test many CRSs simultaneously enabled us to identify a useful set of IL-13-responsive elements. *SPDEFe* was the top regulatory element to respond to IL-13 in a cell type-selective manner in our subsequent validation experiments. *SPDEFe* mutation analyses, including saturation mutagenesis MPRA, allowed us to identify key sequences

involved in the function of this enhancer. Mutations within two STAT6 and three KLF5 motifs perturbed enhancer activity. Cell type specificity could not be explained by a global difference in IL-13 signaling because another STAT6-binding enhancer, *IGHEe*, conferred robust IL-13-responsive transcription in all cell types we studied.

Our results are consistent with a model where IL-13 stimulation triggers STAT6 activation, recruitment of STAT6 and KLF5, and subsequent KLF5-mediated H3K27ac. Reported mechanisms of target gene activation by KLF5 include interaction with transcription factor IIB (TFIIB) and TATA-box-binding protein, other transcriptional coregulators, and post-translational modifiers, including HDAC1/2 and p300.[53] *KLF5* expression and function may help account for differences in enhancer activity between cell types because KLF5 knockdown has been shown to reduce *MUC5AC* expression in esophageal adenocarcinoma[54] and lung epithelial cell lines,[17] and we found modestly higher levels of *KLF5* mRNA in secretory cells compared with basal and ciliated cells. It is also plausible that other secretory cell-specific *trans*-factors interact with KLF5 or STAT6. Previous reports of IL-4 effects on macrophages found functional interaction between STAT6 and another Kruppel-like factor, KLF4, at the *Arg1* promoter[55] and enrichment of STAT6 and KLF motifs in IL-4-induced enhancers.[56] Direct or indirect interactions between STAT6 and KLF family members may therefore be of more general importance in IL-4 and IL-13 signaling.

CRT is a powerful therapeutic tool that can modulate gene expression for beneficial purposes. Utilizing CRISPRi to directly target *SPDEFe*, we were able to show *SPDEF* to be the target gene of this enhancer and to ameliorate asthma-associated phenotypes, including SPDEF-dependent goblet cell metaplasia, pathological mucus production, and mucostasis. Targeting the *SPDEF* promoter (−350 to +130 of the TSS) with repressors of KRAB or methyltransferases has been shown to reduce *SPDEF* expression and downstream mucus-related genes in lung epithelial cell lines.[57] In contrast, our *SPDEFe*-based approach was developed and tested in primary cells differentiated in ALI culture, which more closely models the *in vivo* state[25] and, unlike promoter-based approaches, provides selectivity for cell type (secretory cells) and stimulus (IL-13). Suppressing IL-13-induced goblet cell metaplasia and *MUC5AC* overexpression would likely be beneficial for preventing airway obstruction in asthma, but global suppression of goblet cells and *SPDEF* and *MUC5AC* expression might be deleterious for host defense. Various approaches, including cell type-specific CRISPR-Cas9 delivery vehicles,[58] transcript-specific riboswitches,[59] and miRNA-responsive switches,[60] can be useful for targeting CRISPR-based systems to specific cell types. As an alternative, we used a simple two-component system comprised of a cell type-selective enhancer to control production of KRAB-dCas9 and a sgRNA directed against the *SPDEF* promoter. Using this system, we efficiently suppressed IL-13-induced goblet cell production in a human primary cell culture model. Using a different gRNA against *MUC5AC* promoter allowed us to target this critical downstream gene without disrupting *SPDEF* expression. By using an enhancer that is not activated by other stimuli that promote *SPDEF* and *MUC5AC* expression (PneumaCult-ALI medium and IL-1β), our approach selectively suppresses only IL-13-driven pathology. Unlike dupilumab, a US Food and Drug Administration (FDA)-approved therapeutic agent that blocks IL-4Rα and globally inhibits IL-4 and IL-13,[61] the enhancer-based approach is designed for secretory cell-selective targeting of specific pathogenic genes and could provide durable benefits when introduced into basal progenitor cells in the airway epithelium. Incorporating cell type-selective, cytokine-responsive regulatory circuits could be a simple and powerful tool for highly selective treatment of human diseases.

Limitations of the study

We tested only a portion of the sequences in the IL-13-regulated regions identified in the H3K27ac ChIP-seq experiments; more experiments would be required to test the activity of other sequences in these regions. A caveat of MPRAs is that sequences are tested out of context. Future studies utilizing large-scale CRISPRi screens[62–64] could test large sets of CRSs to identify additional regulatory elements that drive cell type-selective responses to IL-13 and other cytokines. Although we provide evidence of involvement of STAT6 and KLF5 in the secretory cell-selective IL-13 response, questions about the mechanism remain. We were unable to directly test whether STAT6 binds to *SPDEFe* because of lack of suitable antibodies, so we cannot exclude the possibility that the requirement for STAT6 in activation of *SPDEFe* is indirect. Our studies were performed late, 7 days after addition of IL-13, and more studies will be required to determine the sequence of events that drives cell-specific cytokine responses in this system. Finally, our studies were performed in an *ex vivo* cell model, and additional experiments would be necessary to verify the safety and efficacy of enhancer-based therapeutic approaches *in vivo*.

STAR★METHODS

Detailed methods are provided in the online version of this paper and include the following:

- KEY RESOURCES TABLE
- RESOURCE AVAILABILITY
  - Lead contact
  - Materials availability
  - Data and code availability
- EXPERIMENTAL MODEL AND SUBJECT DETAILS
  - Primary cell culture
  - Cell lines
- METHOD DETAILS
  - Plasmids
  - Lentivirus preparation
  - Bulk RNA-seq
  - Single cell RNA-seq
  - H3K27ac ChIP-seq
  - CRISPRi targeting of genomic regulatory elements
  - Quantification of mRNA transcripts
  - Quantification of MUC5AC-positive cells
  - Immunofluorescence staining
  - Measurement of mucociliary transport
  - Lentiviral GFP-based enhancer reporter assay
  - Massively parallel reporter assays

- CRISPR-based gene targeting
- CUT&Tag
- Enhancer-driven CRISPRi targeting

- QUANTIFICATION AND STATISTICAL ANALYSIS

SUPPLEMENTAL INFORMATION

Supplemental information can be found online at https://doi.org/10.1016/j.xgen.2022.100229.

ACKNOWLEDGMENTS

We thank Michael Matthay and Paul Wolters (UCSF) for supplying human bronchial specimens and Jane Gordon, Sarah Elmes (UCSF Laboratory for Cell Analysis), Kari Herrington (UCSF Nikon Imaging Center), Eric Chow (UCSF Center for Advanced Technology), Siranoosh Ashtari (UC Davis DNA Technologies & Expression Analysis Core Laboratory), Luke Gilbert (UCSF), and Jonathan Weissman (MIT) for technical advice and assistance. This work was supported in part by National Institute of Health grants U19 AI077439 (to D.J.E.), R35 HL145235 (to D.J.E. and N.A. with a Diversity Supplement to K.L.H.), R01 HL117004 (to N.A.), and K99/R00 HL135404 (to W.L.E.); Sandler Foundation Program for Breakthrough Biomedical Research Postdoctoral Independent Research award 7028238 (to L.R.B.); and National Natural Science Foundation of China grant 81970016 (to X.Z.).

AUTHOR CONTRIBUTIONS

K.D.K., L.R.B., W.L.E., N.A., and D.J.E. contributed to study conception and design. K.D.K., L.R.B., O.Y.-B., X.Z., K.L.H., D.I.S., and L.T.Z. performed experiments. K.D.K., L.R.B., W.L.E., J.S., O.Y.-B., and X.Z. analyzed data. K.D.K., L.R.B., W.L.E., and D.J.E. interpreted data. W.E.F., N.A., and D.J.E. supervised study execution. K.D.K. and L.R.B. drafted the manuscript. K.D.K., L.R.B., W.L.E., J.S., O.Y.-B., X.Z., K.L.H., D.I.S., L.T.Z., W.E.F., N.A., and D.J.E. revised the manuscript.

DECLARATION OF INTERESTS

K.D.K. (Genentech), L.R.B. (AstraZeneca), and J.S. (Genentech) have additional affiliations as employees. N.A. is the cofounder and a member of the scientific advisory board of Regel Therapeutics and receives funding from BioMarin Pharmaceutical Inc.

Received: May 18, 2022
Revised: October 2, 2022
Accepted: November 14, 2022
Published: December 7, 2022

REFERENCES

1. Vos, T., Lim, S.S., Abbafati, C., Abbas, K.M., Abbasi, M., Abbasifard, M., Abbasi-Kangevari, M., Abbastabar, H., Abd-Allah, F., Abdelalim, A., et al. (2020). Global burden of 369 diseases and injuries in 204 countries and territories, 1990-2019: a systematic analysis for the Global Burden of Disease Study 2019. Lancet *396*, 1204–1222. https://doi.org/10.1016/S0140-6736(20)30925-9.
2. Woodruff, P.G., Modrek, B., Choy, D.F., Jia, G., Abbas, A.R., Ellwanger, A., Koth, L.L., Arron, J.R., and Fahy, J.V. (2009). T-helper type 2-driven inflammation defines major subphenotypes of asthma. Am. J. Respir. Crit. Care Med. *180*, 388–395. https://doi.org/10.1164/rccm.200903-0392OC.
3. Choy, D.F., Hart, K.M., Borthwick, L.A., Shikotra, A., Nagarkar, D.R., Siddiqui, S., Jia, G., Ohri, C.M., Doran, E., Vannella, K.M., et al. (2015). TH2 and TH17 inflammatory pathways are reciprocally regulated in asthma. Sci. Transl. Med. *7*, 301ra129. https://doi.org/10.1126/scitranslmed.aab3142.
4. Bhakta, N.R., Christenson, S.A., Nerella, S., Solberg, O.D., Nguyen, C.P., Choy, D.F., Jung, K.L., Garudadri, S., Bonser, L.R., Pollack, J.L., et al. (2018). IFN-Stimulated gene expression, type 2 inflammation, and endoplasmic reticulum stress in asthma. Am. J. Respir. Crit. Care Med. *197*, 313–324. https://doi.org/10.1164/rccm.201706-1070OC.
5. Wills-Karp, M., Luyimbazi, J., Xu, X., Schofield, B., Neben, T.Y., Karp, C.L., and Donaldson, D.D. (1998). Interleukin-13: central mediator of allergic asthma. Science *282*, 2258–2261. https://doi.org/10.1126/science.282.5397.2258.
6. Grünig, G., Warnock, M., Wakil, A.E., Venkayya, R., Brombacher, F., Rennick, D.M., Sheppard, D., Mohrs, M., Donaldson, D.D., Locksley, R.M., and Corry, D.B. (1998). Requirement for IL-13 independently of IL-4 in experimental asthma. Science *282*, 2261–2263.
7. Farghaly, H.S.M., Blagbrough, I.S., Medina-Tato, D.A., and Watson, M.L. (2008). Interleukin 13 increases contractility of murine tracheal smooth muscle by a phosphoinositide 3-kinase p110delta-dependent mechanism. Mol. Pharmacol. *73*, 1530–1537. https://doi.org/10.1124/mol.108.045419.
8. Kraft, M., Lewis, C., Pham, D., and Chu, H.W. (2001). IL-4, IL-13, and dexamethasone augment fibroblast proliferation in asthma. J. Allergy Clin. Immunol. *107*, 602–606. https://doi.org/10.1067/mai.2001.113760.
9. Kuperman, D.A., Huang, X., Koth, L.L., Chang, G.H., Dolganov, G.M., Zhu, Z., Elias, J.A., Sheppard, D., and Erle, D.J. (2002). Direct effects of interleukin-13 on epithelial cells cause airway hyperreactivity and mucus overproduction in asthma. Nat. Med. *8*, 885–889. https://doi.org/10.1038/nm734.
10. Kuperman, D.A., Huang, X., Nguyenvu, L., Hölscher, C., Brombacher, F., and Erle, D.J. (2005). IL-4 receptor signaling in Clara cells is required for allergen-induced mucus production. J. Immunol. *175*, 3746–3752. https://doi.org/10.4049/jimmunol.175.6.3746.
11. Bonser, L.R., Zlock, L., Finkbeiner, W., and Erle, D.J. (2016). Epithelial tethering of MUC5AC-rich mucus impairs mucociliary transport in asthma. J. Clin. Invest. *126*, 2367–2371. https://doi.org/10.1172/JCI84910.
12. Chen, G., Korfhagen, T.R., Xu, Y., Kitzmiller, J., Wert, S.E., Maeda, Y., Gregorieff, A., Clevers, H., and Whitsett, J.A. (2009). SPDEF is required for mouse pulmonary goblet cell differentiation and regulates a network of genes associated with mucus production. J. Clin. Invest. *119*, 2914–2924. https://doi.org/10.1172/JCI39731.
13. Koh, K.D., Siddiqui, S., Cheng, D., Bonser, L.R., Sun, D.I., Zlock, L.T., Finkbeiner, W.E., Woodruff, P.G., and Erle, D.J. (2020). Efficient RNP-directed human gene targeting reveals SPDEF is required for IL-13-induced mucostasis. Am. J. Respir. Cell Mol. Biol. *62*, 373–381. https://doi.org/10.1165/rcmb.2019-0266OC.
14. Heinz, S., Romanoski, C.E., Benner, C., and Glass, C.K. (2015). The selection and function of cell type-specific enhancers. Nat. Rev. Mol. Cell Biol. *16*, 144–154. https://doi.org/10.1038/nrm3949.
15. Creyghton, M.P., Cheng, A.W., Welstead, G.G., Kooistra, T., Carey, B.W., Steine, E.J., Hanna, J., Lodato, M.A., Frampton, G.M., Sharp, P.A., et al. (2010). Histone H3K27ac separates active from poised enhancers and predicts developmental state. Proc. Natl. Acad. Sci. USA *107*, 21931–21936. https://doi.org/10.1073/pnas.1016071107.
16. Czimmerer, Z., Daniel, B., Horvath, A., Rückerl, D., Nagy, G., Kiss, M., Peloquin, M., Budai, M.M., Cuaranta-Monroy, I., Simandi, Z., et al. (2018). The transcription factor STAT6 mediates direct repression of inflammatory enhancers and limits activation of alternatively polarized macrophages. Immunity *48*, 75–90.e6. https://doi.org/10.1016/j.immuni.2017.12.010.
17. Paranjapye, A., NandyMazumdar, M., Browne, J.A., Leir, S.-H., and Harris, A. (2021). Krüppel-like factor 5 regulates wound repair and the innate immune response in human airway epithelial cells. J. Biol. Chem. *297*, 100932. https://doi.org/10.1016/j.jbc.2021.100932.
18. Qiao, Y., Wang, Z., Tan, F., Chen, J., Lin, J., Yang, J., Li, H., Wang, X., Sali, A., Zhang, L., and Zhong, G. (2020). Enhancer reprogramming within pre-existing topologically associated domains promotes TGF-β-induced EMT

and cancer metastasis. Mol. Ther. *28*, 2083–2095. https://doi.org/10.1016/j.ymthe.2020.05.026.

19. Fossum, S.L., Mutolo, M.J., Tugores, A., Ghosh, S., Randell, S.H., Jones, L.C., Leir, S.-H., and Harris, A. (2017). Ets homologous factor (EHF) has critical roles in epithelial dysfunction in airway disease. J. Biol. Chem. *292*, 10938–10949. https://doi.org/10.1074/jbc.M117.775304.
20. Inoue, F., and Ahituv, N. (2015). Decoding enhancers using massively parallel reporter assays. Genomics *106*, 159–164. https://doi.org/10.1016/j.ygeno.2015.06.005.
21. Matharu, N., and Ahituv, N. (2020). Modulating gene regulation to treat genetic disorders. Nat. Rev. Drug Discov. *19*, 757–775. https://doi.org/10.1038/s41573-020-0083-7.
22. Jackson, N.D., Everman, J.L., Chioccioli, M., Feriani, L., Goldfarbmuren, K.C., Sajuthi, S.P., Rios, C.L., Powell, R., Armstrong, M., Gomez, J., et al. (2020). Single-cell and population transcriptomics reveal pan-epithelial remodeling in type 2-high asthma. Cell Rep. *32*, 107872. https://doi.org/10.1016/j.celrep.2020.107872.
23. McErlean, P., Kelly, A., Dhariwal, J., Kirtland, M., Watson, J., Ranz, I., Smith, J., Saxena, A., Cousins, D.J., Van Oosterhout, A., et al. (2020). Profiling of H3K27Ac reveals the influence of asthma on the epigenome of the airway epithelium. Front. Genet. *11*, 585746. https://doi.org/10.3389/fgene.2020.585746.
24. Bonser, L.R., Koh, K.D., Johansson, K., Choksi, S.P., Cheng, D., Liu, L., Sun, D.I., Zlock, L.T., Eckalbar, W.L., Finkbeiner, W.E., and Erle, D.J. (2021). Flow-cytometric analysis and purification of airway epithelial-cell subsets. Am. J. Respir. Cell Mol. Biol. *64*, 308–317. https://doi.org/10.1165/rcmb.2020-0149MA.
25. Pezzulo, A.A., Starner, T.D., Scheetz, T.E., Traver, G.L., Tilley, A.E., Harvey, B.-G., Crystal, R.G., McCray, P.B., and Zabner, J. (2011). The air-liquid interface and use of primary cell cultures are important to recapitulate the transcriptional profile of in vivo airway epithelia. Am. J. Physiol. Lung Cell Mol. Physiol. *300*, L25–L31. https://doi.org/10.1152/ajplung.00256.2010.
26. Nagasaki, T., Schuyler, A.J., Zhao, J., Samovich, S.N., Yamada, K., Deng, Y., Ginebaugh, S.P., Christenson, S.A., Woodruff, P.G., Fahy, J.V., et al. (2022). 15LO1 dictates glutathione redox changes in asthmatic airway epithelium to worsen type 2 inflammation. J. Clin. Invest. *132*, e151685. https://doi.org/10.1172/JCI151685.
27. Travaglini, K.J., Nabhan, A.N., Penland, L., Sinha, R., Gillich, A., Sit, R.V., Chang, S., Conley, S.D., Mori, Y., Seita, J., et al. (2020). A molecular cell atlas of the human lung from single-cell RNA sequencing. Nature *587*, 619–625. https://doi.org/10.1038/s41586-020-2922-4.
28. Guo, M., Tomoshige, K., Meister, M., Muley, T., Fukazawa, T., Tsuchiya, T., Karns, R., Warth, A., Fink-Baldauf, I.M., Nagayasu, T., et al. (2017). Gene signature driving invasive mucinous adenocarcinoma of the lung. EMBO Mol. Med. *9*, 462–481. https://doi.org/10.15252/emmm.201606711.
29. Rada-Iglesias, A., Bajpai, R., Prescott, S., Brugmann, S.A., Swigut, T., and Wysocka, J. (2012). Epigenomic annotation of enhancers predicts transcriptional regulators of human neural crest. Cell Stem Cell *11*, 633–648. https://doi.org/10.1016/j.stem.2012.07.006.
30. Bonser, L.R., Eckalbar, W.L., Rodriguez, L., Shen, J., Koh, K.D., Zlock, L.T., Christenson, S., Woodruff, P.G., Finkbeiner, W.E., and Erle, D.J. (2021). The Type 2 Asthma Mediator IL-13 Inhibits SARS-CoV-2 Infection of Bronchial Epithelium. https://doi.org/10.1101/2021.02.25.432762.
31. Ostuni, R., Piccolo, V., Barozzi, I., Polletti, S., Termanini, A., Bonifacio, S., Curina, A., Prosperini, E., Ghisletti, S., and Natoli, G. (2013). Latent enhancers activated by stimulation in differentiated cells. Cell *152*, 157–171. https://doi.org/10.1016/j.cell.2012.12.018.
32. Nakada, E.M., Bhakta, N.R., Korwin-Mihavics, B.R., Kumar, A., Chamberlain, N., Bruno, S.R., Chapman, D.G., Hoffman, S.M., Daphtary, N., Aliyeva, M., et al. (2019). Conjugated bile acids attenuate allergen-induced airway inflammation and hyperresponsiveness by inhibiting UPR transducers. JCI Insight *4*, 98101. https://doi.org/10.1172/jci.insight.98101.
33. Rajavelu, P., Chen, G., Xu, Y., Kitzmiller, J.A., Korfhagen, T.R., and Whitsett, J.A. (2015). Airway epithelial SPDEF integrates goblet cell differentiation and pulmonary Th2 inflammation. J. Clin. Invest. *125*, 2021–2031. https://doi.org/10.1172/JCI79422.
34. Forno, E., Zhang, R., Jiang, Y., Kim, S., Yan, Q., Ren, Z., Han, Y.-Y., Boutaoui, N., Rosser, F., Weeks, D.E., et al. (2020). Transcriptome-wide and differential expression network analyses of childhood asthma in nasal epithelium. J. Allergy Clin. Immunol. *146*, 671–675. https://doi.org/10.1016/j.jaci.2020.02.005.
35. Herr, W., and Clarke, J. (1986). The SV40 enhancer is composed of multiple functional elements that can compensate for one another. Cell *45*, 461–470. https://doi.org/10.1016/0092-8674(86)90332-6.
36. Khan, A., Fornes, O., Stigliani, A., Gheorghe, M., Castro-Mondragon, J.A., van der Lee, R., Bessy, A., Chèneby, J., Kulkarni, S.R., Tan, G., et al. (2018). JASPAR 2018: update of the open-access database of transcription factor binding profiles and its web framework. Nucleic Acids Res. *46*, D260–D266. https://doi.org/10.1093/nar/gkx1126.
37. Junttila, I.S. (2018). Tuning the cytokine responses: an update on interleukin (IL)-4 and IL-13 receptor complexes. Front. Immunol. *9*, 888. https://doi.org/10.3389/fimmu.2018.00888.
38. Gordon, M.G., Inoue, F., Martin, B., Schubach, M., Agarwal, V., Whalen, S., Feng, S., Zhao, J., Ashuach, T., Ziffra, R., et al. (2020). lentiMPRA and MPRAflow for high-throughput functional characterization of gene regulatory elements. Nat. Protoc. *15*, 2387–2412. https://doi.org/10.1038/s41596-020-0333-5.
39. Synthego (2019). Synthego Performance Analysis, ICE Analysis (Synthego).
40. Wan, H., Luo, F., Wert, S.E., Zhang, L., Xu, Y., Ikegami, M., Maeda, Y., Bell, S.M., and Whitsett, J.A. (2008). Kruppel-like factor 5 is required for perinatal lung morphogenesis and function. Development *135*, 2563–2572. https://doi.org/10.1242/dev.021964.
41. Kaya-Okur, H.S., Wu, S.J., Codomo, C.A., Pledger, E.S., Bryson, T.D., Henikoff, J.G., Ahmad, K., and Henikoff, S. (2019). CUT&Tag for efficient epigenomic profiling of small samples and single cells. Nat. Commun. *10*, 1930. https://doi.org/10.1038/s41467-019-09982-5.
42. Kanai, A., Suzuki, K., Tanimoto, K., Mizushima-Sugano, J., Suzuki, Y., and Sugano, S. (2011). Characterization of STAT6 target genes in human B cells and lung epithelial cells. DNA Res. *18*, 379–392. https://doi.org/10.1093/dnares/dsr025.
43. Messner, B., Stütz, A.M., Albrecht, B., Peiritsch, S., and Woisetschläger, M. (1997). Cooperation of binding sites for STAT6 and NF kappa B/rel in the IL-4-induced up-regulation of the human IgE germline promoter. J. Immunol. *159*, 3330–3337.
44. Leung, C., Wadsworth, S.J., Yang, S.J., and Dorscheid, D.R. (2020). Structural and functional variations in human bronchial epithelial cells cultured in air-liquid interface using different growth media. Am. J. Physiol. Lung Cell Mol. Physiol. *318*, L1063–L1073. https://doi.org/10.1152/ajplung.00190.2019.
45. Chen, G., Sun, L., Kato, T., Okuda, K., Martino, M.B., Abzhanova, A., Lin, J.M., Gilmore, R.C., Batson, B.D., O'Neal, Y.K., et al. (2019). IL-1β dominates the promucin secretory cytokine profile in cystic fibrosis. J. Clin. Invest. *129*, 4433–4450. https://doi.org/10.1172/JCI125669.
46. Stuart, W.D., Guo, M., Fink-Baldauf, I.M., Coleman, A.M., Clancy, J.P., Mall, M.A., Lim, F.-Y., Brewington, J.J., and Maeda, Y. (2020). CRISPRi-mediated functional analysis of lung disease-associated loci at non-coding regions. NAR Genom. Bioinform. *2*, lqaa036. https://doi.org/10.1093/nargab/lqaa036.
47. Dixit, A., Parnas, O., Li, B., Chen, J., Fulco, C.P., Jerby-Arnon, L., Marjanovic, N.D., Dionne, D., Burks, T., Raychowdhury, R., et al. (2016). Perturb-seq: dissecting molecular circuits with scalable single-cell RNA profiling of pooled genetic screens. Cell *167*, 1853–1866.e17. https://doi.org/10.1016/j.cell.2016.11.038.

48. Chen, G., Volmer, A.S., Wilkinson, K.J., Deng, Y., Jones, L.C., Yu, D., Bustamante-Marin, X.M., Burns, K.A., Grubb, B.R., O'Neal, W.K., et al. (2018). Role of spdef in the regulation of Muc5b expression in the airways of naive and mucoobstructed mice. Am. J. Respir. Cell Mol. Biol. *59*, 383–396. https://doi.org/10.1165/rcmb.2017-0127OC.

49. ENCODE Project Consortium (2012). An integrated encyclopedia of DNA elements in the human genome. Nature *489*, 57–74. https://doi.org/10.1038/nature11247.

50. Heinz, S., Texari, L., Hayes, M.G.B., Urbanowski, M., Chang, M.W., Givarkes, N., Rialdi, A., White, K.M., Albrecht, R.A., Pache, L., et al. (2018). Transcription elongation can affect genome 3D structure. Cell *174*, 1522–1536.e22. https://doi.org/10.1016/j.cell.2018.07.047.

51. Larose, M.-C., Chakir, J., Archambault, A.-S., Joubert, P., Provost, V., Laviolette, M., and Flamand, N. (2015). Correlation between CCL26 production by human bronchial epithelial cells and airway eosinophils: involvement in patients with severe eosinophilic asthma. J. Allergy Clin. Immunol. *136*, 904–913. https://doi.org/10.1016/j.jaci.2015.02.039.

52. Gordon, E.D., Sidhu, S.S., Wang, Z.-E., Woodruff, P.G., Yuan, S., Solon, M.C., Conway, S.J., Huang, X., Locksley, R.M., and Fahy, J.V. (2012). A protective role for periostin and TGF-β in IgE-mediated allergy and airway hyperresponsiveness. Clin. Exp. Allergy *42*, 144–155. https://doi.org/10.1111/j.1365-2222.2011.03840.x.

53. Diakiw, S.M., D'Andrea, R.J., and Brown, A.L. (2013). The double life of KLF5: opposing roles in regulation of gene-expression, cellular function, and transformation. IUBMB Life *65*, 999–1011. https://doi.org/10.1002/iub.1233.

54. Ng, C.K., Ma, K., Cheng, Y., Miyashita, T., Harmon, J.W., and Meltzer, S.J. (2019). Krüppel-like factor 5 promotes sonic hedgehog signaling and neoplasia in barrett's esophagus and esophageal adenocarcinoma. Transl. Oncol. *12*, 1432–1441. https://doi.org/10.1016/j.tranon.2019.07.006.

55. Liao, X., Sharma, N., Kapadia, F., Zhou, G., Lu, Y., Hong, H., Paruchuri, K., Mahabeleshwar, G.H., Dalmas, E., Venteclef, N., et al. (2011). Krüppel-like factor 4 regulates macrophage polarization. J. Clin. Invest. *121*, 2736–2749. https://doi.org/10.1172/JCI45444.

56. Hoeksema, M.A., Shen, Z., Holtman, I.R., Zheng, A., Spann, N.J., Cobo, I., Gymrek, M., and Glass, C.K. (2021). Mechanisms underlying divergent responses of genetically distinct macrophages to IL-4. Sci. Adv. *7*, eabf9808. https://doi.org/10.1126/sciadv.abf9808.

57. Song, J., Cano-Rodriquez, D., Winkle, M., Gjaltema, R.A.F., Goubert, D., Jurkowski, T.P., Heijink, I.H., Rots, M.G., and Hylkema, M.N. (2017). Targeted epigenetic editing of SPDEF reduces mucus production in lung epithelial cells. Am. J. Physiol. Lung Cell Mol. Physiol. *312*, L334–L347. https://doi.org/10.1152/ajplung.00059.2016.

58. Alyami, M.Z., Alsaiari, S.K., Li, Y., Qutub, S.S., Aleisa, F.A., Sougrat, R., Merzaban, J.S., and Khashab, N.M. (2020). Cell-type-specific CRISPR/Cas9 delivery by biomimetic metal organic frameworks. J. Am. Chem. Soc. *142*, 1715–1720. https://doi.org/10.1021/jacs.9b11638.

59. Liu, Y., Zhan, Y., Chen, Z., He, A., Li, J., Wu, H., Liu, L., Zhuang, C., Lin, J., Guo, X., et al. (2016). Directing cellular information flow via CRISPR signal conductors. Nat. Methods *13*, 938–944. https://doi.org/10.1038/nmeth.3994.

60. Hirosawa, M., Fujita, Y., and Saito, H. (2019). Cell-type-specific CRISPR activation with MicroRNA-responsive AcrIIA4 switch. ACS Synth. Biol. *8*, 1575–1582. https://doi.org/10.1021/acssynbio.9b00073.

61. Harb, H., and Chatila, T.A. (2020). Mechanisms of dupilumab. Clin. Exp. Allergy *50*, 5–14. https://doi.org/10.1111/cea.13491.

62. Gasperini, M., Hill, A.J., McFaline-Figueroa, J.L., Martin, B., Kim, S., Zhang, M.D., Jackson, D., Leith, A., Schreiber, J., Noble, W.S., et al. (2019). A genome-wide framework for mapping gene regulation via cellular genetic screens. Cell *176*, 377–390.e19. https://doi.org/10.1016/j.cell.2018.11.029.

63. Fulco, C.P., Munschauer, M., Anyoha, R., Munson, G., Grossman, S.R., Perez, E.M., Kane, M., Cleary, B., Lander, E.S., and Engreitz, J.M. (2016). Systematic mapping of functional enhancer-promoter connections with CRISPR interference. Science *354*, 769–773. https://doi.org/10.1126/science.aag2445.

64. Li, K., Liu, Y., Cao, H., Zhang, Y., Gu, Z., Liu, X., Yu, A., Kaphle, P., Dickerson, K.E., Ni, M., and Xu, J. (2020). Interrogation of enhancer function by enhancer-targeting CRISPR epigenetic editing. Nat. Commun. *11*, 485. https://doi.org/10.1038/s41467-020-14362-5.

65. Love, M.I., Huber, W., and Anders, S. (2014). Moderated estimation of fold change and dispersion for RNA-seq data with DESeq2. Genome Biol. *15*, 550. https://doi.org/10.1186/s13059-014-0550-8.

66. Ritchie, M.E., Phipson, B., Wu, D., Hu, Y., Law, C.W., Shi, W., and Smyth, G.K. (2015). Limma powers differential expression analyses for RNA-sequencing and microarray studies. Nucleic Acids Res. *43*, e47. https://doi.org/10.1093/nar/gkv007.

67. Van der Auwera, G.A., Carneiro, M.O., Hartl, C., Poplin, R., Del Angel, G., Levy-Moonshine, A., Jordan, T., Shakir, K., Roazen, D., Thibault, J., et al. (2013). From FastQ data to high confidence variant calls: the Genome Analysis Toolkit best practices pipeline. Curr. Protoc. Bioinformatics *43*, 11.10.1–11.10.33. https://doi.org/10.1002/0471250953.bi1110s43.

68. Hafemeister, C., and Satija, R. (2019). Normalization and variance stabilization of single-cell RNA-seq data using regularized negative binomial regression. Genome Biol. *20*, 296. https://doi.org/10.1186/s13059-019-1874-1.

69. Finak, G., McDavid, A., Yajima, M., Deng, J., Gersuk, V., Shalek, A.K., Slichter, C.K., Miller, H.W., McElrath, M.J., Prlic, M., et al. (2015). MAST: a flexible statistical framework for assessing transcriptional changes and characterizing heterogeneity in single-cell RNA sequencing data. Genome Biol. *16*, 278. https://doi.org/10.1186/s13059-015-0844-5.

70. Ma, Y., Sun, S., Shang, X., Keller, E.T., Chen, M., and Zhou, X. (2020). Integrative differential expression and gene set enrichment analysis using summary statistics for scRNA-seq studies. Nat. Commun. *11*, 1585. https://doi.org/10.1038/s41467-020-15298-6.

71. Dobin, A., Davis, C.A., Schlesinger, F., Drenkow, J., Zaleski, C., Jha, S., Batut, P., Chaisson, M., and Gingeras, T.R. (2013). STAR: ultrafast universal RNA-seq aligner. Bioinformatics *29*, 15–21. https://doi.org/10.1093/bioinformatics/bts635.

72. Heinz, S., Benner, C., Spann, N., Bertolino, E., Lin, Y.C., Laslo, P., Cheng, J.X., Murre, C., Singh, H., and Glass, C.K. (2010). Simple combinations of lineage-determining transcription factors prime cis-regulatory elements required for macrophage and B cell identities. Mol. Cell *38*, 576–589. https://doi.org/10.1016/j.molcel.2010.05.004.

73. Ershov, D., Phan, M.-S., Pylvänäinen, J.W., Rigaud, S.U., Le Blanc, L., Charles-Orszag, A., Conway, J.R.W., Laine, R.F., Roy, N.H., Bonazzi, D., et al. (2022). TrackMate 7: integrating state-of-the-art segmentation algorithms into tracking pipelines. Nat. Methods *19*, 829–832. https://doi.org/10.1038/s41592-022-01507-1.

74. Zhang, Y., Liu, T., Meyer, C.A., Eeckhoute, J., Johnson, D.S., Bernstein, B.E., Nusbaum, C., Myers, R.M., Brown, M., Li, W., and Liu, X.S. (2008). Model-based analysis of ChIP-seq (MACS). Genome Biol. *9*, R137. https://doi.org/10.1186/gb-2008-9-9-r137.

75. Horani, A., Nath, A., Wasserman, M.G., Huang, T., and Brody, S.L. (2013). Rho-associated protein kinase inhibition enhances airway epithelial basal-cell proliferation and lentivirus transduction. Am. J. Respir. Cell Mol. Biol. *49*, 341–347. https://doi.org/10.1165/rcmb.2013-0046TE.

76. Adamson, B., Norman, T.M., Jost, M., Cho, M.Y., Nuñez, J.K., Chen, Y., Villalta, J.E., Gilbert, L.A., Horlbeck, M.A., Hein, M.Y., et al. (2016). A multiplexed single-cell CRISPR screening platform enables systematic dissection of the unfolded protein response. Cell *167*, 1867–1882.e21. https://doi.org/10.1016/j.cell.2016.11.048.

77. Zhao, W., Pollack, J.L., Blagev, D.P., Zaitlen, N., McManus, M.T., and Erle, D.J. (2014). Massively parallel functional annotation of 3' untranslated regions. Nat. Biotechnol. *32*, 387–391. https://doi.org/10.1038/nbt.2851.

78. Inoue, F., Kircher, M., Martin, B., Cooper, G.M., Witten, D.M., McManus, M.T., Ahituv, N., and Shendure, J. (2017). A systematic comparison reveals substantial differences in chromosomal versus episomal encoding of enhancer activity. Genome Res. *27*, 38–52. https://doi.org/10.1101/gr.212092.116.

79. Gilbert, L.A., Horlbeck, M.A., Adamson, B., Villalta, J.E., Chen, Y., Whitehead, E.H., Guimaraes, C., Panning, B., Ploegh, H.L., Bassik, M.C., et al. (2014). Genome-scale CRISPR-mediated control of gene repression and activation. Cell *159*, 647–661. https://doi.org/10.1016/j.cell.2014.09.029.

80. Levin, M.H., Sullivan, S., Nielson, D., Yang, B., Finkbeiner, W.E., and Verkman, A.S. (2006). Hypertonic saline therapy in cystic fibrosis: evidence against the proposed mechanism involving aquaporins. J. Biol. Chem. *281*, 25803–25812. https://doi.org/10.1074/jbc.M604332200.

81. Christenson, S.A., van den Berge, M., Faiz, A., Inkamp, K., Bhakta, N., Bonser, L.R., Zlock, L.T., Barjaktarevic, I.Z., Barr, R.G., Bleecker, E.R., et al. (2019). An airway epithelial IL-17A response signature identifies a steroid-unresponsive COPD patient subgroup. J. Clin. Invest. *129*, 169–181. https://doi.org/10.1172/JCI121087.

82. Zheng, G.X.Y., Terry, J.M., Belgrader, P., Ryvkin, P., Bent, Z.W., Wilson, R., Ziraldo, S.B., Wheeler, T.D., McDermott, G.P., Zhu, J., et al. (2017). Massively parallel digital transcriptional profiling of single cells. Nat. Commun. *8*, 14049. https://doi.org/10.1038/ncomms14049.

83. Kang, H.M., Subramaniam, M., Targ, S., Nguyen, M., Maliskova, L., McCarthy, E., Wan, E., Wong, S., Byrnes, L., Lanata, C.M., et al. (2018). Multiplexed droplet single-cell RNA-sequencing using natural genetic variation. Nat. Biotechnol. *36*, 89–94. https://doi.org/10.1038/nbt.4042.

84. Stuart, T., Butler, A., Hoffman, P., Hafemeister, C., Papalexi, E., Mauck, W.M., Hao, Y., Stoeckius, M., Smibert, P., and Satija, R. (2019). Comprehensive integration of single-cell data. Cell *177*, 1888–1902.e21. https://doi.org/10.1016/j.cell.2019.05.031.

85. Butler, A., Hoffman, P., Smibert, P., Papalexi, E., and Satija, R. (2018). Integrating single-cell transcriptomic data across different conditions, technologies, and species. Nat. Biotechnol. *36*, 411–420. https://doi.org/10.1038/nbt.4096.

86. Mak, A.C.Y., White, M.J., Eckalbar, W.L., Szpiech, Z.A., Oh, S.S., Pino-Yanes, M., Hu, D., Goddard, P., Huntsman, S., Galanter, J., et al. (2018). Whole-genome sequencing of pharmacogenetic drug response in racially diverse children with asthma. Am. J. Respir. Crit. Care Med. *197*, 1552–1564. https://doi.org/10.1164/rccm.201712-2529OC.

87. Li, Q., Brown, J.B., Huang, H., and Bickel, P.J. (2011). Measuring reproducibility of high-throughput experiments. Ann. Appl. Stat. *5*, 1752–1779. https://doi.org/10.1214/11-AOAS466.

88. Amemiya, H.M., Kundaje, A., and Boyle, A.P. (2019). The ENCODE blacklist: identification of problematic regions of the genome. Sci. Rep. *9*, 9354. https://doi.org/10.1038/s41598-019-45839-z.

89. Inoue, F., Eckalbar, W.L., Wang, Y., Murphy, K.K., Matharu, N., Vaisse, C., and Ahituv, N. (2019). Genomic and epigenomic mapping of leptin-responsive neuronal populations involved in body weight regulation. Nat. Metab. *1*, 475–484. https://doi.org/10.1038/s42255-019-0051-x.

90. Quinlan, A.R., and Hall, I.M. (2010). BEDTools: a flexible suite of utilities for comparing genomic features. Bioinformatics *26*, 841–842. https://doi.org/10.1093/bioinformatics/btq033.

91. Perez, A.R., Pritykin, Y., Vidigal, J.A., Chhangawala, S., Zamparo, L., Leslie, C.S., and Ventura, A. (2017). GuideScan software for improved single and paired CRISPR guide RNA design. Nat. Biotechnol. *35*, 347–349. https://doi.org/10.1038/nbt.3804.

92. Kircher, M., Xiong, C., Martin, B., Schubach, M., Inoue, F., Bell, R.J.A., Costello, J.F., Shendure, J., and Ahituv, N. (2019). Saturation mutagenesis of twenty disease-associated regulatory elements at single base-pair resolution. Nat. Commun. *10*, 3583. https://doi.org/10.1038/s41467-019-11526-w.

STAR★METHODS

KEY RESOURCES TABLE

REAGENT or RESOURCE	SOURCE	IDENTIFIER
Antibodies		
Anti-Histone H3K27ac (rabbit polyclonal)	Abcam	Cat# ab4729; RRID: AB_2118291
Anti-MUC5AC (45M1) [DyLight 405] (mouse monoclonal)	Novus Biologicals	Cat# NBP2-32732V
Anti-MUC5AC (45M1) [DyLight 488] (mouse monoclonal)	Novus Biologicals	Cat# NBP2-32732G
Anti-MUC5AC (45M1) (mouse monoclonal)	Thermo Fisher Scientific	Cat# MA5-12178; RRID: AB_10978001
Anti-MUC5B (rabbit polyclonal)	Millipore Sigma	Cat# HPA008246; RRID: AB_1854203
Anti-ac-α-Tubulin (6–11B-1) (mouse monoclonal)	Santa Cruz Biotechnology	Cat# sc-23950; RRID: AB_628409
Rhodamine Red-X anti-mouse IgG (Fcγ subclass 2b) (goat polyclonal)	Jackson ImmunoResearch Laboratories	Cat# 115-295-207; RRID: AB_2338771
Alexa Fluor 488 anti-mouse IgG (Fcγ subclass 1) (goat polyclonal)	Jackson ImmunoResearch Laboratories	Cat# 115-545-205; RRID: AB_2338854
Alexa Fluor 647 anti-rabbit IgG (H + L) (goat polyclonal)	Jackson ImmunoResearch Laboratories	Cat# 111-605-144; RRID: AB_2338078
Anti-CD271 (ME20.4–1.H4) [APC] (mouse monoclonal)	Miltenyi Biotec	Cat# 130-113-418; RRID: AB_2733363
Anti-CD66c (B6.2) [Brilliant Violet 421] (mouse monoclonal)	BD Biosciences	Cat# 742683; RRID: AB_2740965
Anti-ac-α-Tubulin (6–11B-1) [Alexa Fluor 647] (mouse monoclonal)	Santa Cruz Biotechnology	Cat# sc-23950AF647; RRID: AB_628409
Anti-KLF5 (rabbit polyclonal)	Abcam	Cat# ab137676; RRID: AB_2744553
Biological samples		
HBECs	UC San Francisco	N/A
Chemicals, peptides, and recombinant proteins		
Y-27632	Enzo Life Sciences	Cat# ALX-270-333
Recombinant human IFN-a	R&D Systems	Cat# 11100–1
Recombinant human IL-13	PeproTech	Cat# 200–13
Recombinant human IL-17	PeproTech	Cat# 200–17
Recombinant human IL-1b	PeproTech	Cat# 200–01B
BEGM Bronchial Epithelial Cell Growth Medium BulletKit	Lonza	Cat# CC-3170
PneumaCult-ALI Medium	STEMCELL Technologies	Cat# 05001
PowerUp SYBR Green Master Mix	Thermo Fisher Scientific	Cat# A25741
Recombinant Cas9-NLS	MacroLabs	N/A
Collagen from human placenta	Millipore Sigma	Cat# C7521
Critical commercial assays		
Chromium Next GEM Single Cell 3′ Kit v3.1	10x Genomics	Cat# PN-1000268
LowCell# ChIP kit protein A	Diagenode	Cat# kch-maglow-A16
Hyperactive pA-Tn5 In-Situ ChIP Library Prep Kit	Vazyme Biotech	Cat# TD901
Deposited data		
Bulk RNA-seq data	GEO	GSE185200
scRNA-seq data	GEO	GSE185199
H3K27ac ChIP-seq data	GEO	GSE185201
KLF5 CUT&Tag data	GEO	GSE183433
Experimental models: Cell lines		
BEAS-2B	ATCC	Cat# CRL-9609; RRID: CVCL_0168
A549	ATCC	Cat# CCL-185
Lenti-X 293T	Clontech	Cat# 632180

(*Continued on next page*)

Continued

REAGENT or RESOURCE	SOURCE	IDENTIFIER
Oligonucleotides		
RT-qPCR primers (See Table S4)	IDT	N/A
Synthetic sgRNAs (See Table S3)	Synthego	N/A
Software and algorithms		
DESeq2	Love et al.[65]	N/A
LIMMA	Ritchie et al.[66]	N/A
10x Genomics Cell Ranger	10x Genomics	N/A
GATK	Van der Auwera et al.[67]	N/A
Sctransform	Hafemeister and Satija[68]	N/A
MAST	Finak et al.[69]	N/A
iDEA	Ma et al.[70]	N/A
STAR (v2.5.2b)	Dobin et al.[71]	N/A
HOMER	Heinz et al.[72]	N/A
TrackMate	Ershov et al.[73]	N/A
FlowJo	FlowJo	N/A
MPRAflow	Gordon et al.[38]	N/A
MACS2	Zhang et al.[74]	N/A
GraphPad Prism	GraphPad	N/A
Custom code	GitHub: https://github.com/janeshen91/HBEC_cytokine_data_scripts	Zenodo: https://doi.org/10.5281/zenodo.7300394

RESOURCE AVAILABILITY

Lead contact

Further information and requests for resources and reagents should be directed to and will be fulfilled by the lead contact, David J. Erle (david.erle@ucsf.edu).

Materials availability

Plasmids generated in this study are available from the lead contact upon request.

Data and code availability

Bulk RNA-seq, scRNA-seq, H3K27ac ChIP-seq, and KLF5 CUT&Tag data have been deposited at Gene Expression Omnibus (GEO) and are publicly available. Accession numbers are listed in the key resources table.

All original code has been deposited at Zenodoub: https://doi.org/10.5281/zeno and GitHub: https://github.com/janeshen91/HBEC_cytokine_data_scripts and is publicly available. DOIs are listed in the key resources table.

Any additional information required to reanalyze the data reported in this paper is available from the lead contact upon request.

EXPERIMENTAL MODEL AND SUBJECT DETAILS

Primary cell culture

The UCSF Committee on Human Research approved the use of HBECs isolated from lung transplant recipients' explanted lungs or lungs not used for transplantation. Written consent was not required since materials were leftover clinical samples obtained from de-identified individuals (sex unknown as a result). HBECs were seeded onto 10-cm dishes coated with human placental collagen (HPC; Sigma-Aldrich, St. Louis, MO) and propagated in BEGM (Lonza, Walkersville, MD) with 10 μM Y-27632 (Enzo Life Sciences, Farmingdale, NY) as described previously.[13,75]

Cell lines

BEAS-2B and A549 cells were cultured in 1:1 DMEM/F12 medium containing Non-Essential Amino Acids (Genesee Scientific, San Diego, CA) and DMEM, respectively, with 10% FBS (Thermo Fisher Scientific, Waltham, MA).

METHOD DETAILS

Plasmids

Plasmid hU6-sgRNA-cr3-EF1a-Puro was made by cloning in hU6-sgRNA-cr3-EF1a-Puro construct from pMJ117[76] (a gift from J. Weissman lab at MIT) into XhoI,XbaI-cut (New England BioLabs, Ipswich, MA) backbone of BTV.[77] Plasmid EF1a-dCas9-KRAB-P2A-BSD was made by cloning in EF1a-dCas9, KRAB from IGI-P0152 (a gift from J. Corn lab at ETH Zurich via L. Gilbert lab at UCSF), P2A-BSD from pLenti-SFFV-KRAB-dCas9-P2A-BSD into XhoI,XbaI-cut backbone of BTV. Plasmid mP-KRAB-dCas9_EF1a-BSD was made by cloning in SV40 poly(A) signal from BTV, BSD, EF1a from lentiCRISPRv2, antirepressor#40-mP from pLS-mP,[78] and KRAB-dCas9 from pHR-TRE3G-KRAB-dCas9-P2A-mCherry[79] (a gift from L. Gilbert lab) into XhoI,XbaI-cut backbone of BTV. NEBuilder HiFi DNA Assembly (New England BioLabs) was used for cloning.

Lentivirus preparation

Third generation lentivirus was produced by transfecting appropriate plasmids or plasmid libraries with three lentivirus-packaging plasmids (pMDL, pVSV-G, and pRSV-Rev) into HEK293T cells using TransIT-293 Transfection Reagent (Mirus Bio, Madison, WI). Harvested lentivirus was concentrated 100-fold using Lenti-X Concentrator (Takara Bio, Mountain View, CA), resuspended in PBS, and stored at −80°C in aliquots.

Bulk RNA-seq

HBECs from six donors (1 = 12–43, 2 = 13–26, 3 = 13–33, 4 = 13–24, 5 = 13–23, and 6 = 13–28) were cultured at ALI for 23 d, as described previously,[13,80] without cytokine or with IFN-α (10 ng/mL for the final 1 d), IFN-γ (10 ng/mL for the final 1 d), IL-13 (10 ng/mL for the final 7 d), IL-17 (10 ng/mL for the final 7 d), or the combination of IFN-α and IL-13. We elected to use six donors (more than the typical 3–4 used in similar experiments) to determine whether the responses to cytokines were consistent. The principal component analyses, together with the finding of large numbers of significant cytokine-induced gene expression changes, indicate that effects were consistent and that the experiment was powered adequately to detect thousands of genes regulated by each cytokine treatment. Interferons and interleukins were acquired from R&D Systems (Minneapolis, MN) and Peprotech (Rocky Hill, NJ), respectively. After removal of accumulated mucus with 10 mM dithiothreitol (DTT; Enzo Life Sciences, Farmingdale, NY) in PBS, cells were trypsinized with 0.25% trypsin-EDTA (Thermo Fisher Scientific) for 10–15 min at 37°C and neutralized. RNA was isolated from harvested HBECs, and bulk RNA-seq was performed as previously described.[4,81] We have previously reported other analyses based upon a subset of these data from unstimulated cells and cells stimulated with IFN-α[4] and IL-17.[81] In addition, data for 332 genes associated with SARS-CoV-2 have been reported in another study.[30] Raw read counts per sample and gene were used as input to DESeq2[65] for unsupervised and supervised analysis. Read counts were first normalized for sequencing depth and transformed using DESeq2's variance stabilizing transformation. Donor specific impacts on the stabilized counts where then removed with LIMMA's removeBatchEffect function.[66] The major sources of variability where then inspected with a principal component analysis (PCA) using the top 3000 most variable genes across the experiment. Differential gene expression in response to each cytokine treatment compared to untreated was then determined using DESeq2 after correction for the donor specific effects using the design formula: ~ donor + condition, where condition includes all treatment options, IFN-α, IFN-γ, IL-13, IL-17, and the combination of IFN-α and IL-13. Pairwise comparisons between treatments and the untreated control were carried out with DESeq2 results function using a Wald test to estimate p-value and a multiple testing correction using the FDR method.

Single cell RNA-seq

We used HBECs from four (1 = 12–43, 2 = 13–26, 3 = 13–33, and 6 = 13–28) of the six donors used for bulk RNA-seq. Cells were cultured at ALI for 23 d without cytokine or with IFN-α (10 ng/mL for the final 1 d), IL-13 (10 ng/mL for the final 7 d), IL-17 (10 ng/mL for the final 7 d), or the combination of IFN-α and IL-13. Given the consistency of bulk RNA-seq, we elected to use four donors for scRNA-seq and were again able to identify large numbers of differentially expressed genes. Single cell suspensions were generated as described above. Cells were manually counted using a hemocytometer, and equal numbers of cells from each donor were pooled. Each pool included four samples (one from each donor and each representing a different cytokine stimulation). 10x Genomics scRNA-seq libraries (Pleasanton, CA) were prepared[82] and sequenced using Illumina NovaSeq 6000 S4 flow cells (San Diego, CA) at the Center for Advanced Technology at UCSF. Resulting sequence reads were processed into a cell-by-gene counts matrix using 10x Genomics Cell Ranger software. Single nucleotide polymorphisms that were unique to one of the four donors were identified from the bulk RNA-seq data following the GATK best practices[67] and used to assign each cell to the appropriate donor using Demuxlet.[83] Demultiplexed droplets uniquely assigned to a single individual were then processed using Seurat[84,85] with the following filters: nFeature_RNA >= 500 & nFeature_RNA <7500 & nCount_RNA >1200 & percent.mito <0.5 & percent.ribo <0.35. The top 10,000 variable genes were carried forward for normalization, unsupervised clustering, UMAP visualization, and cell type identification. Normalized data was scaled while regressing out the 10x Genomics well effect, percent mitochondrial reads, percent ribosomal reads, and the number of unique molecular indexes per cell. Cells from cultures that were not stimulated with cytokines were then isolated for clustering and cell type identification. These unstimulated cells then served as the reference dataset for Seurat's reference-based multiple dataset integration using SCTransform[68] with label transfer in order to use anchor genes from the unstimulated cells to identify cell types across all samples. Cell identities were then returned to the original Seurat object prior to

SCTransform for further investigation. We used Seurat's FindAllMarkers to identify cell type marker genes. To find genes that have cell-type-specific responses to cytokine stimulation, we used the package MAST.[69] A hurdle model was fitted with the covariates batch, individual and cngeneson (a MAST-specific covariate that corrects for cellular detection rate), cell type, and cell type by cytokine interaction terms. Significance testing using the lrt() function was used to find differentially expressed genes by cytokine stimulation as compared to untreated genes in the same cell type. Data for 332 genes associated with SARS-CoV-2 infection have been reported in another study.[30] For linear model cell type interaction analysis, we downsampled the number of cells in basal, ciliated, and secretory cells to 450 cells each, to minimize the effect of sample size on power of detecting differentially expressed genes. The same hurdle model with covariates for batch, individual and cngeneson, cell type, and cell type by cytokine interaction terms was fitted. Genes with p-value for cell type by cytokine interaction terms <0.1 were called significant. Gene set enrichment analysis was performed using the package iDEA[70] and Gene Ontology Biological Process (GOBP) gene sets from Msigdb ("c5.go.bp.v7.4.symbols.gmt"). We used the default parameters from the function iDEA.fit, except that the minimum number of DE genes was set to 2. Log_2 fold change and p-values from MAST-based differential gene expression were used as input.

H3K27ac ChIP-seq

H3K27ac ChIP-seq was performed on three of the donors used in sequencing studies (1 = 12–43, 2 = 13–26, and 6 = 13–28) and one additional donor 16–05. Given the consistency of bulk RNA-seq, we elected to use four donors for ChIP-seq and were again able to identify large numbers of changes in H3K27ac. HBECs were cultured at ALI for 23 d without cytokine or with IFN-α (10 ng/mL for the final 1 d), IL-13 (10 ng/mL for the final 7 d), or IL-17 (10 ng/mL for the final 7 d). ChIP-seq was performed using previously reported methods.[86] In brief, cells were harvested, fixed with 0.5% paraformaldehyde (PFA; Thermo Fisher Scientific), and lysed, and then chromatin was sheared using a Covaris S2 sonicator (Woburn, MA). Chromatin immunoprecipitation was performed with an H3K27ac antibody (ab4729, rabbit IgG; Abcam, Cambridge, UK) using the Diagenode LowCell# ChIP kit (Denville, NJ) as per the manufacturer's instructions. Libraries were prepared using the Rubicon DNA-seq kit (Rubicon Genomics, Atlanta, GA) and then sequenced on an Illumina HiSeq 4000 using 50-bp single end at the Center for Advanced Technology at UCSF. Sequencing reads were aligned by STAR v2.5.2b[83], and reproducible peaks were called for each condition using the ENCODE IDR framework.[87] Additionally, regions blacklisted by the ENCODE consortium[88] for their tendency to produce anomalous results were removed from the peak set using bedtools. Analysis for differentially enriched peaks in response to cytokines was carried out as previously described.[89] Differentially modulated peaks were inspected for proximity to differentially expressed genes from bulk and single cell RNA-seq data using Bedtools v2.29.2.[90] HOMER motif analysis (http://homer.ucsd.edu/homer/introduction/programs.html)[72] was performed on upregulated and downregulated H3K27ac peaks with parameter size –given. Peaks with p-value > 0.1 was used as background peaks.

CRISPRi targeting of genomic regulatory elements

Each gRNA sequence (Table S3) was selected using CRISPick (https://portals.broadinstitute.org/gppx/crispick/public) and GuideScan[91] and was used to design a pair of complementary 5′-phosphorylated oligonucleotides (5′-PO_4-ATGNNNNN NNNNNNNNNNNNNNNGTTTCAGAGC-3′ and 5′-PO_4-TTAGCTCTGAAACNNNNNNNNNNNNNNNNNNNNCATGTTT-3′; where Ns indicate sequences that vary according to the gRNA). A G was added to the 5′ ends of gRNA sequences not beginning with a G. gRNA oligonucleotides (oligos; IDT, San Jose, CA) were annealed and cloned into the hU6-sgRNA-cr3-EF1a-Puro plasmid digested with BstXI and BlpI (New England Biolabs). HBECs were initially transduced with EF1a-dCas9-KRAB-P2A-BSD lentivirus and maintained in BEGM with 10 μM Y-27632 and 10 μg/mL blasticidin (Thermo Fisher Scientific) for 3 d for selection. Cells were subsequently transduced with sgRNA lentivirus and maintained in BEGM with 10 μM Y-27632, 10 μg/mL blasticidin, and 1 μg/mL puromycin (Thermo Fisher Scientific) for 3 d for selection. Transduced and selected cells were then passaged to Transwell inserts for culture at ALI for 23 d. Where indicated, IL-13 (10 ng/mL) was added for the final 7 d of culture.

Quantification of mRNA transcripts

mRNAs were measured by quantitative real-time RT-PCR (qRT-PCR). RNA was extracted from HBECs using the RNeasy Mini Kit (QIAGEN, Hilden, Germany) or the RNA/DNA/Protein Purification Plus Kit (Norgen Biotek, Thorold, ON, Canada) according to manufacturers' instructions. RNA was reverse-transcribed using SuperScript III First-Strand Synthesis System (Thermo Fisher Scientific). cDNA was analyzed by qRT-PCR (PowerUp SYBR Green, Thermo Fisher Scientific; primer sequences in Table S4). The mean value of three technical replicates was used for analysis. mRNA levels were normalized to *GAPDH* levels, and comparisons were made using the ΔΔCt method.

Quantification of MUC5AC-positive cells

MUC5AC-positive HBECs were quantified as described previously.[13] Either anti-MUC5AC-DL488 or anti-MUC5AC-DL405 (45M1, mouse IgG_1; Novus Biologicals, Centennial, CO) antibody was used. Flow cytometry (FACS Canto II, BD Biosciences, San Jose, CA) was performed at UCSF Laboratory for Cell Analysis, and data analysis was done with FlowJo (FlowJo LLC, Ashland, OR). The threshold for MUC5AC-positive cells was established based on staining of IL-13-treated cells with an isotype control antibody (<0.5% of isotype control-stained cells exceeded the threshold).

Immunofluorescence staining

Paraffin-embedded microscopic sections and whole mounts of HBEC culture Transwell inserts were prepared as described previously.[11] Immunofluorescence staining was done with following primary antibodies: mouse monoclonal anti-MUC5AC (45M1; Thermo Fisher Scientific; 1:200), rabbit polyclonal anti-MUC5B (H-300, sc-20119; Santa Cruz Biotechnology, Dallas, TX; 1:200), and mouse monoclonal anti acetylated alpha tubulin (6–11B-1, sc-23950; Santa Cruz Biotechnology; 1:200). After washing, slides were incubated with appropriate secondary antibodies (Rhodamine goat anti-mouse, Alex Fluor 647 goat anti-rabbit, and Alexa Fluor 488 goat anti-mouse; Jackson ImmunoResearch Laboratories) at 1:200 dilution for 1 h. 4′,6-diamidinio-2-phenylindole (DAPI, 1:1000) was used to stain nuclei. Immunofluorescence images were acquired using a Yokagawa CSU22 spinning-disk confocal microscope connected to a Nikon Ti-E at Nikon Imaging Center and Center for Advanced Light Microscopy at UCSF. Slides were placed on the microscope stage and fluorescence and brightfield images were acquired using a 20X objective. Identical acquisition settings were used throughout each experiment. Images were processed using Fiji.

Measurement of mucociliary transport

Mucociliary transport was measured as described previously.[11,13] Briefly, 2-μm yellow-green (505/515) fluorescent microspheres (Thermo Fisher Scientific) were applied to the apical surface of HBEC cultures with intact mucus gels and allowed to disperse for 5 min. Cultures were then transferred to an optical cell dish (MatTek, Ashland, MA) and placed on the stage of a spinning disc confocal microscope under a dry 10X objective at 37°C with perfluorocarbon (Sigma-Aldrich). Transport of fluorescent microspheres was imaged in the plane of the gel by recording sequential images every 1 s over 1 min. Images were analyzed using the TrackMate plugin in Fiji.[73] Median microsphere speed was determined for each of three fields from one well per condition for each of three donors.

Lentiviral GFP-based enhancer reporter assay

Enhancer test sequences (Table S5) were PCR-amplified from genomic DNA of BEAS-2B cells or synthesized (IDT, Newark, NJ) and cloned into XbaI and SbfI sites of the lentiviral GFP-based enhancer reporter plasmid pLS-mP[78] using the Quick Ligation Kit or NEBuilder HIFI Assembly (New England Biolabs, Ipswich, MA), respectively. For mutations in STAT6 and KLF5 binding sites, we substituted every nucleotide within the consensus binding motif without changing the length of the sequence. HBECs were seeded at ~25% confluence in HPC-coated Transwell inserts (Corning, Corning, NY) and transduced with lentivirus. Transduced cells were maintained in ALI medium with 10 mM Y-27632 until 100% confluence and cultured at ALI for 23 d. Where indicated, PneumaCult-ALI Medium (STEMCELL Technologies, Vancouver, Canada) was used during the ALI culture, IL-13 (10 ng/mL) or IL-1β (10 ng/mL) were added to the culture medium for the final 7 d of the culture period. Cells were harvested, fixed in 4% PFA for 10 min at 4°C, washed with PBS, and resuspended in eBioScience Flow Cytometry Staining Buffer (Thermo Fisher Scientific). GFP level was assessed by flow cytometry (FACSCanto II; BD Biosciences, San Jose, CA). In experiments assessing GFP levels in different subsets of HBECs, cells were blocked with 5% normal goat serum (Jackson ImmunoResearch Laboratories) and either stained with anti-NGFR/CD271-APC (ME20.4, mIgG$_1$; BioLegend, San Diego, CA) and anti-CEACAM6/CD66c-BV421 (B6.2, mIgG$_1$; BD Biosciences, San Jose, CA) antibodies to separate basal and secretory cells, or permeablized with 0.2% Saponin (Sigma-Aldrich, St. Louis, MO) and stained with anti-acetylated-α-tubulin-AF647 (6–11B-1, mIgG$_{2b}$; Santa Cruz Biotechnology, Dallas, TX) antibody to separate ciliated cells.[24] In experiments with undifferentiated HBECs, BEAS-2B, and A549 cells, cells were seeded at ~25% confluence in HPC-coated or intact 12-well plates, transduced with lentivirus, and maintained in appropriate growth medium for 6 d post-transduction. Where indicated, IL-13 (10 ng/mL) was added to the culture medium for the final 4 d.

Massively parallel reporter assays

Enhancer MPRAs, including saturation mutagenesis MPRA, were done as described previously[92] with minor modifications. For the saturation mutagenesis MPRA, all 600 possible single nucleotide variants of *SPDEFe*(1–200) were designed in addition to the wild-type, reference sequence and control sequences which included scrambled, SV40e, and IGHEe sequences, resulting in total of 638 sequences. For H3K27ac ChIP-seq-based MPRA, 1,904 CRSs were designed in addition to the control sequences which included scrambled, SV40e, and *SPDEFe*(1–200) sequences. MPRAs were done with two donors and at least 30 barcodes associated with each sequence (providing a form of internal replication); data correlated well between the two donors and we were able to detect even modest effects with high statistical significance. A pool of 230-nt oligos containing each of these 200-nt sequences flanked by 15-nt primer recognition sequences was synthesized (SurePrint Oligonucleotide Libraries; Agilent Technologies, Santa Clara, CA), amplified, and cloned into the MPRA plasmid. Briefly, inserts were amplified and cloned upstream of a minimal promoter driving an *eGFP* reporter transcript with a barcode (BC). We aimed for ~50 BCs per sequence when constructing the plasmid library. Each insert was associated with a set of BCs using paired-end customized NGS (see Gordon et al. Step 83[38]). All MPRA-related sequencing was performed using an Illumina NextSeq 500 by the DNA Technologies & Expression Analysis Core Laboratory at UC Davis. 250,000 cells from each of two HBEC donors were transduced at a multiplicity of infection of 4, passaged to HPC-coated Transwell inserts, maintained in ALI medium with 10 mM Y-27632 until 100% confluence, and cultured at ALI for 23 d. Where indicated, IL-13 (10 ng/mL) was added to the culture medium for the final 7 d of culture. ~5,000,000 cells from each donor was harvested for each condition. Both genomic DNA and RNA were extracted using the AllPrep DNA/RNA mini kit (QIAGEN), and sequencing libraries were generated using a custom library preparation protocol for DNA and RNA extracts. DNA and RNA libraries were sequenced as specified in Gordon et al., Step 161.[38] MPRAflow (https://mpraflow.readthedocs.io/en/latest/quickstart.html) was

used for association and count analysis. Barcode association was done using an amended association workflow, where we filtered for NM = 0, mapq>0, and baseq>30. BCs were then filtered for coverage >3 and uniquely mapped to the enhancer sequence. A linear model.

$$\log2\ \text{RNA count} \sim \log2\ \text{DNA count} + N + \text{intercept}$$

was fitted for each variant enhancer sequence against the wildtype enhancer sequence, where N = 1 for wildtype and N = 0 for the variant sequence. Multiple testing adjustment was done where p-values were adjusted by FDR. Enhancer sequences with FDR <0.05 were considered significant.

CRISPR-based gene targeting

Gene targeting via CRISPR in HBECs was done as described previously.[13] gRNA sequences are listed in Table S2. Synthetic sgRNAs from Synthego (Redwood City, CA) and rCas9 from MacroLabs (Berkeley, CA) were used; nucleofections were performed with the 4D-Nucleofector System (program DC-100; Lonza). Transfected cells were subsequently transduced with lentivirus containing GFP-based enhancer reporter constructs. Cells were then passaged to Transwell inserts for culture at ALI for 23 d. Where indicated, IL-13 (10 ng/mL) was added for the final 7 d of culture. To assess efficiency of gene targeting, genomic DNA was amplified using primers flanking the target sites and analyzed by Sanger sequencing and the Inference of CRISPR Edits (ICE) software tool (Synthego). PCR and sequencing primer sequences are provided in Table S6. For analysis of the efficiency of deletion of an ~0.6 kb region containing *SPDEFe*, genomic DNA was amplified using primers flanking the target sites (Table S6) and amplified DNA was analyzed by agarose gel electrophoresis followed by densitometry to determine the relative abundance of shorter PCR products (*SPDEFe* deleted) and longer PCR products (*SPDEFe* not deleted).

CUT&Tag

HBECs from three donors (10–75, 13–32, and 14–30) cultured at ALI for 23 d. Where indicated, IL-13 (10 ng/mL) was added for the final 7 d of culture. CUT&Tag was performed with 3 donors, 2 replicates per donor, and selected peaks reproduced across replicates (using IDR). CUT&Tag was conducted using a Hyperactive pA-Tn5 In-Situ ChIP Library Prep Kit for Illumina (Vazyme Biotech Co., Nanjing, China) with minor modifications to the manufacturer's protocol as follows. Anti-KLF5 (ab137676, polyclonal rabbit IgG; Abcam) and anti-STAT6 (5397, monoclonal rabbit IgG; Cell Signaling Technology, Danvers, MA) (ab32520, monoclonal rabbit IgG; Abcam) antibodies were used, and normal rabbit IgG was used as a negative control (NI01; Sigma-Aldrich). No secondary antibody was used. The starting cell amount was 500,000 cells, and primary antibody incubation was done overnight. Post-amplification, magnetic bead-based clean-up (HighPrep PCR Clean-up System; MAGBIO Genomics, Gaithersburg, MD) was conducted twice for each clean-up step. We used a small amount of the tagmented and pre-amplified library to set the final number of cycles needed for final library amplification. The cycle threshold (Ct) for which the library had reached 1/3 of its maximal fluorescence (Rn) was set independently for each sample. Libraries were sequenced (paired end 150 bp) using NextSeq (DNA Technologies & Expression Analysis Core Laboratory at UC Davis) and NovaSeq SP 300 (Center for Advanced Technology at UCSF) sequencers. Reads were aligned with STAR with reference hg38. Peaks were called with MACS2 (parameters -f BAM –keep-dup 1 -p 0.01 –nomodel).[74] Overlaps between reproducible peaks were found using IDR. The union of the CUT&Tag peaks with IDR score >540 (or reproducibility <0.05) across the same donor and treatment conditions were combined into one file and used in subsequent analyses. HOMER Motif analysis was performed with parameter size –given. Intersections of peaks from two technical replicates per donor and three donors were used in the differentially modulated peaks analysis. To find peaks modulated by IL-13 stimulation, R package DESEQ2 was used (R version 4.0.1, DESeq2 version 1.28.1). Samtools was used to extract counts from all three donors across two conditions, obtained from the merged bam files of for each donor/treatment condition. Normalization through median of ratios was performed, and a negative binomial GLM was fitted to the count data. Peaks with p-value < 0.1 were called as significantly upregulated or downregulated peaks.

Enhancer-driven CRISPRi targeting

Enhancer sequences (Table S5) were PCR-amplified from genomic DNA from BEAS-2B cells or synthesized (IDT) and cloned into XbaI and SbfI sites of the mP-KRAB-dCas9_EF1a-BSD plasmid using the Quick Ligation Kit or NEBuilder HIFI Assembly. HBECs were initially transduced with enhancer-mP-KRAB-dCas9 lentivirus and maintained in BEGM with 10 μM Y-27632 and 10 μg/mL blasticidin (Thermo Fisher Scientific) for 3 d for selection. Cells were subsequently transduced with sgRNA lentivirus and maintained in BEGM with 10 μM Y-27632, 10 μg/mL blasticidin, and 1 μg/mL puromycin (Thermo Fisher Scientific) for 3 d for selection. Transduced and selected cells were then passaged to Transwell inserts for culture at ALI for 23 d. Where indicated, IL-13 (10 ng/mL) was added for the final 7 d of culture.

QUANTIFICATION AND STATISTICAL ANALYSIS

Each statistical analysis and software/package used is listed either in appropriate method details sections for each high-throughput sequencing method/dataset or in appropriate figure legends for other types of data.